Survey of state-of-the-art NDA methods

Applicable to UF$_6$ cylinders

IAEA task n 07/TAU-04

R. Berndt, E. Franke, P. Mortreau

Mission

The mission of the IPSC is to provide research results and to support EU policy-makers in their effort towards global security and towards protection of European citizens from accidents, deliberate attacks, fraud and illegal actions against EU policies

European Commission
Joint Research Centre
Institute for the Protection and Security of the Citizen

Contact information
Address: TP 800- JRC Ispra- 21020 ISPRA (VA)
E-mail: patricia.mortreau@jrc.it
Tel.: +39 0 332 78 9211
Fax: +39 0 332 78 5073

http://ipsc.jrc.ec.europa.eu/
http://www.jrc.ec.europa.eu/

Legal Notice
Neither the European Commission nor any person acting on behalf of the Commission is responsible for the use which might be made of this publication.

A great deal of additional information on the European Union is available on the Internet.
It can be accessed through the Europa server http://europa.eu/

Requested task and assumptions

In the framework of a project aiming to establish an unattended measurement station at an isotope enrichment facility, IAEA required a study to describe the state of the art of NDA methods applicable to UF_6 cylinders.

The objective of the present work is to provide a feasibility assessment study of all known NDA techniques applicable to the quantitative verification of all uranium categories involved in an enrichment processing plant.

The assay of the UF_6 cylinders covers:

-   the determination of   the enrichment,
-   the confirmation the UF_6 mass (assumed to have been previously weighted by the plant operator and independently verified by inspectors),
-   the assay of the UF_6 homogeneity.

The various hypothesis and practical constraints to be taken into account for the study requirements are [1]:

- the cylinders to be considered are either 30B type (product) or 48Y type (feed and tail),
- the enriched uranium is either from natural origin or reprocessed uranium,
- the cylinders must be assayed at various temperatures,
- the distance between the cylinder and the detector must be at least 50 cm to allow for safe movements of the cylinders,
- the UF_6 mass determination should be accurate within 10% for low enriched uranium, 15% for natural uranium and 20% for depleted uranium,
- the enrichment determination must be given with a total uncertainty which does not exceed:

    - 4.5% for low enriched uranium product,
    - 9.5% for natural uranium,
    - 18% for depleted uranium,

- the measurements have to be performed in 5 minutes and in remote mode to minimize the intrusion on normal plant operator.

With the objectives and assumptions as described above in mind, this document first gives an overview of the radiation properties of UF_6 (chapter A) as well as some practical considerations regarding the 48Y and 30B cylinders (chapter B). The next part reviews the classical NDA methods applicable to UF_6 and refers to intense measurement campaigns carried out in the years 70 -80 (chapter C), whereas the chapter D is dedicated to specific studies involving more recent techniques such as analysis of delayed neutrons and delayed photons.

The most appropriate techniques will be then investigated in chapter E.

The study will be based on our own results of previous measurement campaigns (^{235}U determination with gamma detectors with germanium or LaBr$_3$ detectors) and on MCNP simulations (passive and active neutron methods).

Table of contents

A Radiation characteristics of Uranium hexafluoride

The purpose of this section is to summarize the characteristic gamma rays and neutron radiation from UF_6 and their daughters.

Since alpha and beta particles emitted by the uranium isotopes as well as uranium X-ray cannot cross the thick wall of UF_6 cylinders, the only visible signature comes from gamma and neutron radiation.

A 1. Description of uranium isotopes

Natural Uranium

In its natural state, uranium consists of three isotopes ^{234}U, ^{235}U and ^{238}U. Extremely low quantity of ^{236}U due to activation processes as cosmic ray activation can also be present. Mass spectrometry analysis of U samples collected showed that the isotopic composition of natural uranium varies slightly as a function of its geographical origin. By measuring a set of different U ore, it was shown in [2] showed that the range of natural variation of the three natural isotopes expressed in at% is:

^{234}U	0.0054-0.0051 at%
^{235}U	0.7207-0.7201 at%
^{238}U	99.2748-99.2739 at%

An upper limit for $^{236}U/^{238}U$ of about 6.10^{-10} was found in [2] whereas two U ores originating from Oklo and of the Czech Republic presented a significant presence of ^{236}U ($9.3.10^{-9}$ at% and $2.54.10^{-8}$ at%), thus indicating the presence of neutron processes in these samples.

Reprocessed uranium

In addition to the three naturally occurring Uranium isotopes, the reprocessed Uranium contains all the isotopes from ^{232}U to ^{240}U. Table 1 shows the example of the U isotopic composition of a LWR spent fuel reactor (burn up= 33000.MWD, initial enrichment=3.2%):

U isotope	Half-life	charge	discharge	Discharge		
				Cooling time (year)		
				1	3	6
^{232}U	69.8 a	0.000E+00	2.810E-04	4.248E-04	6.138E-04	7.233E-04
^{233}U	$1.592.10^5$ a	0.000E+00	4.643E-03	4.796E-03	5.118E-03	5.440E-03
^{234}U	$2.457.10^5$ a	2.574E+02	1.163E+02	1.177E+02	1.203E+02	1.230E+02
^{235}U	$7.037.10^8$ a	3.201E+04	7.516E+03	7.516E+03	7.516E+03	7.516E+03
^{236}U	$2.342.10^8$ a	0.000E+00	4.437E+03	4.437E+03	4.438E+03	4.437E+03
^{237}U	6.75 d	0.000E+00	1.021E+01	2.951E-05	2.969E-05	2.450E-05
^{238}U	$4.468.10^9$	9.677E+05	9.434E+05	9.434E+05	9.434E+05	9.434E+05
^{239}U	23.5min	0.000E+00	0.000E+00	0.000E+00	0.000E+00	0.000E+00
^{240}U	14.1 h	2.203E-21	2.203E-21	2.203E-21	2.203E-21	2.203E-21

Table 1: Nuclide concentrations (g/t) of a PWR fuel with a burn up of 33000MWD and an initial Enrichment of 3.2%

The isotopes ^{237}U, ^{239}U and ^{240}U have a very short half life and ^{233}U is present in very small quantities.

Variations of the $^{234}U/^{235}U$ ratio values at different stage of the fuel cycle

The knowledge of the $^{234}U/^{235}U$ ratio is crucial for the passive neutron measurement. It has to be known and ensured to be constant.

During the enrichment process, ^{234}U is preferentially enriched along with ^{235}U, thus increasing the $^{234}U/^{235}U$ ratio whose final value depends on whether the enrichment cascade is designed for low enriched uranium product (power reactor fuel), high enriched uranium product (weapons or naval reactor fuel) and the use of uranium other than natural for feed.

Examples of isotopic composition in AGR UO_2 fuel with 2.207% and 3.42% ^{235}U initial enrichment show that the ratio is equal to 0.00860 and 0.00877 respectively [3] against 0.0075 for natural Uranium.

During the irradiation of the reactor, ^{234}U absorbs a neutron to create ^{235}U and gets burnt gradually. The $^{234}U/^{235}U$ ratio increases and reaches a final value which depends on the burn-up.
In the example of table 1, this ratio which is initially equal to 0.0080 becomes 0.0157 at the end of the irradiation.
During the cooling and storage time, the ^{234}U level increases slightly due to its in-growth from the decay of ^{238}Pu (fig 1). After a cooling time of 3 years, a PWR fuel with a burn up of 33MWD and an initial enrichment of 3.2% has a $^{234}U/^{235}U$ ratio equal to 0.0160.
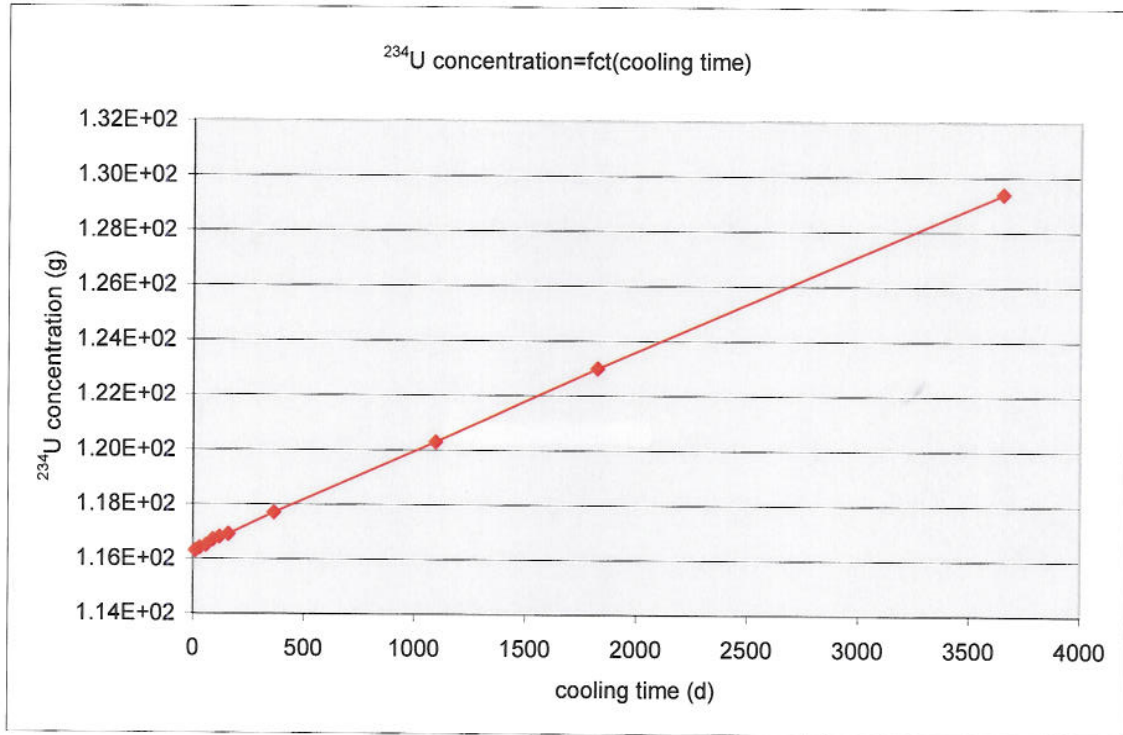
Figure 1: ^{234}U concentrations in spent fuel as a function of the cooling time

For the enrichment of reprocessed uranium, lighter isotopes ^{232}U and ^{234}U reach the top of the cascade before ^{235}U. The relative amount of ^{234}U increases again. Table 2 shows an example of the different value of the ^{234}U/^{235}U for two re-enriched reprocessed uranium.

U isotope	Feed material, origin PWR 900MWe, Burnup 33GWd/t	Re enriched U 3.25 wt%	Re enriched U 5.0 wt%
^{232}U	1.1ppb	4.8ppb	7.6ppb
^{234}U	0.021%wt	0.085%wt	0.133%wt
^{235}U	0.92%wt	3.25%wt	5%wt
^{236}U	0.42%wt	1.09%wt	1.55%wt
^{238}U	98.64%wt	95.25%wt	93.23%wt
^{234}U/^{235}U	0.023	0.026	0.027

Table 2: Isotopic abundances and ^{234}U/^{235}U ratio for re enriched uranium

A 2. Gamma ray spectra

Typical features of U spectra as well as the difference between enriched natural UF_6 and enriched reprocessed uranium are illustrated by figures 2a/2b and figure 3.

Uranium oxide spectra accumulated with a Germanium planar detector are shown in fig 2a and fig 2b. The samples used for the measurement do not contain neither ^{232}U nor ^{233}U but trace amounts of ^{236}U.

Despite of the fact that, these two spectra were measured with U oxide powders, the UF_6 spectra present the same basic characteristics.

Gamma lines in the 80-105 keV region

The 80-105 keV region (fig. 2a) of the U spectrum is characterised by an overlapping of many X and gamma rays which contains the signature from ^{235}U and from ^{231}Th and ^{234}Th, daughter products of ^{235}U and ^{238}U respectively.

The Th Kα-rays (93.35 and 89,96 keV), Pa Kα (95.86 and 92.28 keV), the ^{231}Th gamma lines at 89.95, 99.28, 102.27 keV belong to the decay ^{235}U which present only one weak line at 96.09 keV.
The decay of ^{238}U gives birth to two gamma rays of ^{234}Th at 92.38 and 92.80 keV.

The most intense lines (U kα at 98.43 and 94.65 keV) are due to self fluorescence of the material itself.
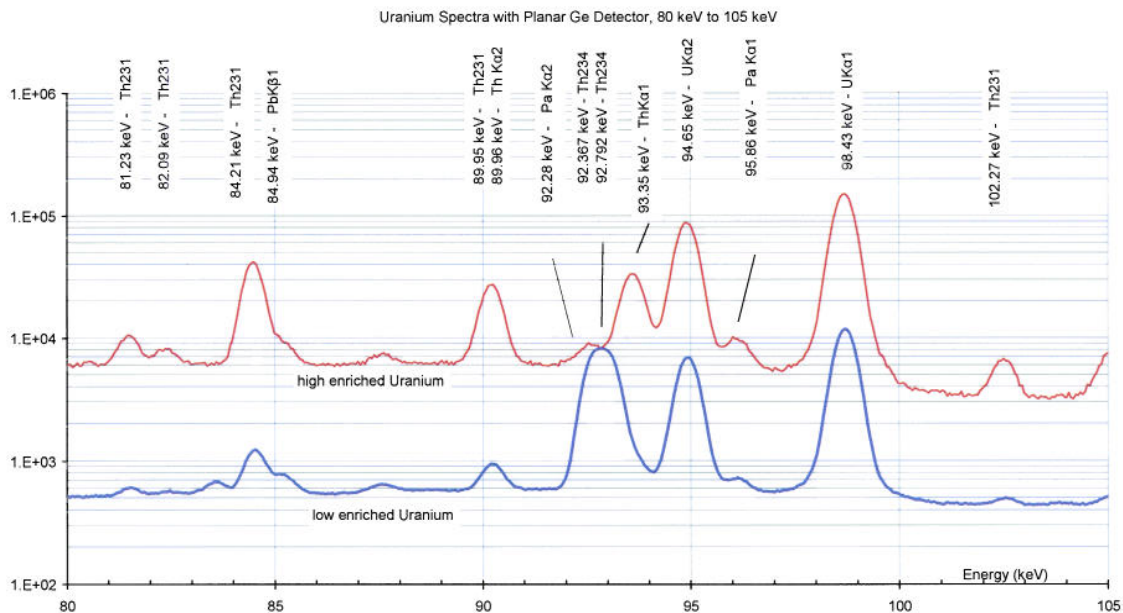
Figure 2a: Uranium spectra taken with a Germanium detector- 80-105 keV region [4]

Gamma lines in the 100-210 keV region

Fig. 2b show the typical lines of ^{235}U including the well known 185.7 keV line.
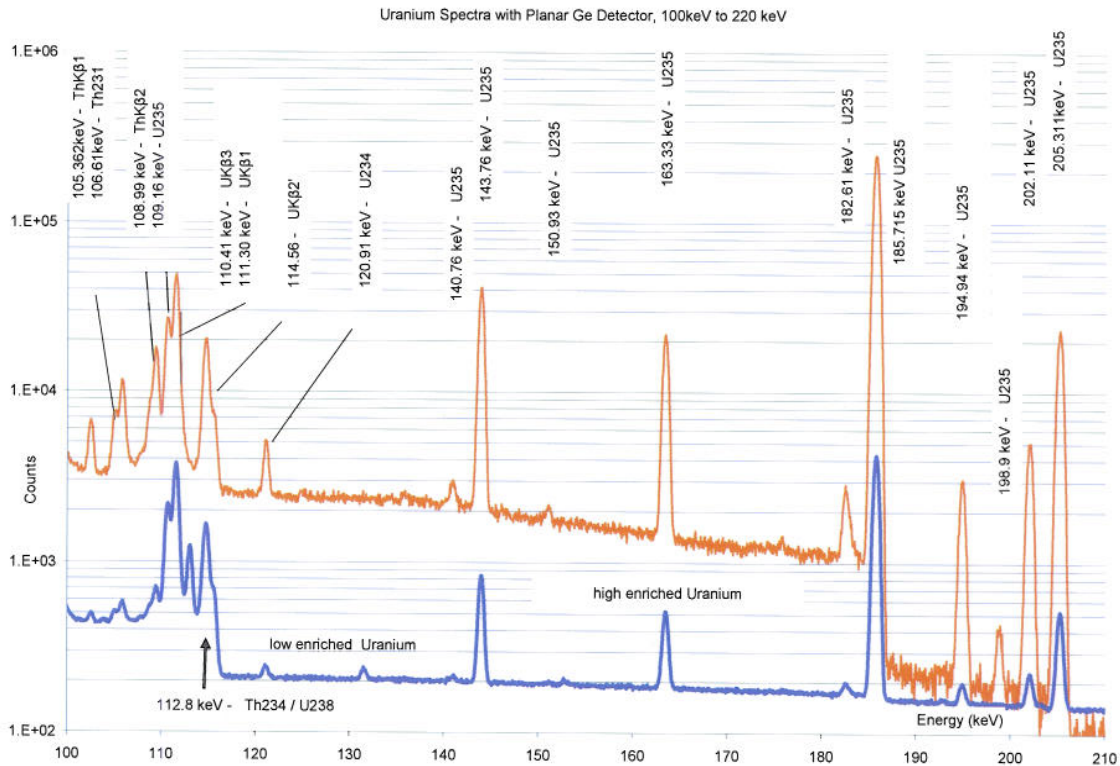
Figure 2b: Uranium spectra taken with a Germanium detector- 100-210 keV region [4]

It is also possible to observe the 120.91 keV of ^{234}U for the samples in thin aluminium containers due to the low absorption in the aluminium containers.

Unfortunately the wall thickness of the 30B and 48Y containers prevents using all these possibilities for characterizing the uranium isotopes.

Gamma lines above 140 keV

Figure 3 shows spectra of depleted natural UF$_6$ and depleted reprocessed uranium stored in 48Y containers. The measurements were performed with a planar Germanium detector in the 50- 2500 keV range.

Compared to fig 1b, the 143 keV and 163 keV of ^{235}U and the 120.9 keV of ^{234}U are not visible anymore due to the strong attenuation in the 16 mm thick steel container.

The 185.7 keV is still enough intense to be used to determine the ^{235}U enrichment with the enrichment meter principle. There is no ^{235}U line above 210 keV.
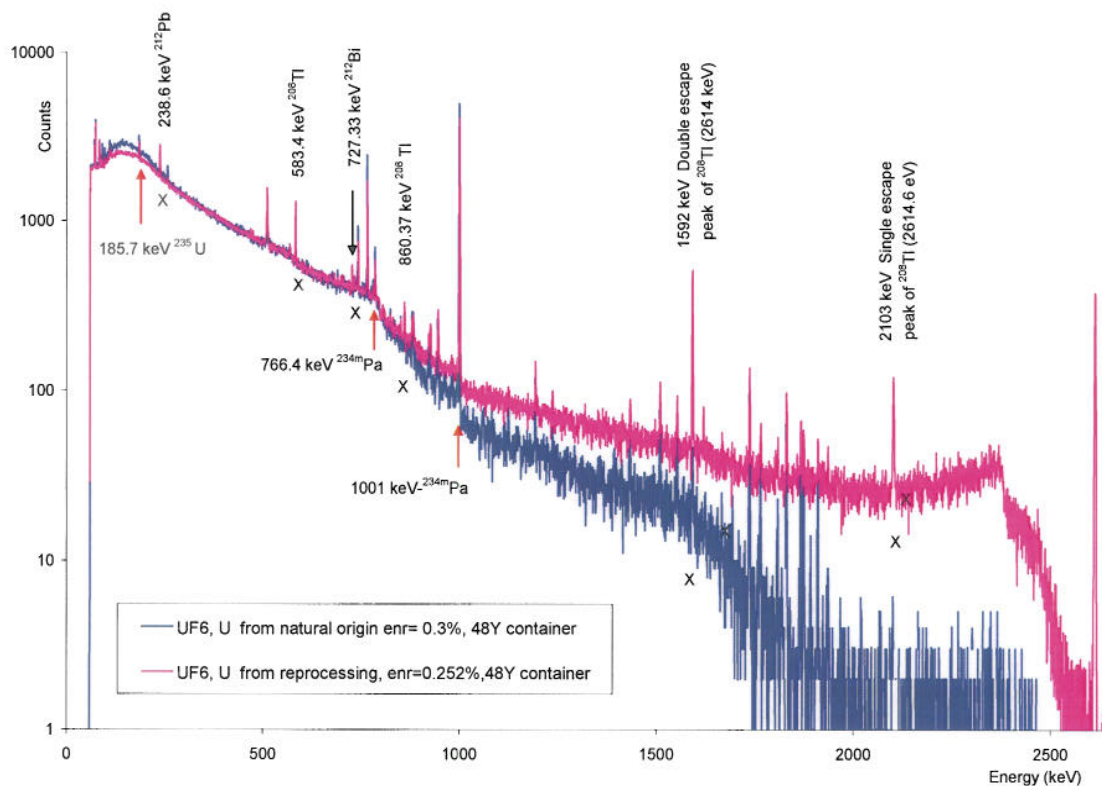
Figure 3: UF$_6$ spectra, from natural or reprocessed uranium

^{238}U is identified with the gamma rays of its daughter nuclides ^{234m}Pa (at 766.4 keV and 1001.0 keV) and ^{234}Pa (880 keV, 883 keV, 925 keV, 926.7 keV). That isotope is in secular equilibrium with ^{238}U after several times of half life (24.1 day of ^{234}Th). Its signature can only be used if the history of the individual drum is known which is not compatible with the use of automated systems

The depleted reprocessed uranium presents several specific lines emitted by the decay products of ^{232}U.
Below 250 keV, the reprocessed uranium can be clearly identified with the 238 keV line of ^{212}Pb. The lines of ^{208}Tl at 583, 860 and 2614.6 keV are typical signature of ^{232}U presence.
The contribution of the scattered radiation of the 2614.6 keV line as well as well as the single and double escape peak associated to this line   also allow identifying the presence of reprocessed material.

Since ^{228}Th is a common decay product of ^{232}U and ^{232}Th decay (see annex 1), the same series of gamma lines can also be observed in the ^{232}Th spectra. Only, the line at 911 keV line produced by ^{228}Ac (decay product of ^{232}Th but of ^{232}U) allows concluding to the presence of ^{232}Th.

Other possible features in UF$_6$ spectrum

The spectra shown in Fig. 3 were measured with depleted UF$_6$. However, when measuring high enriched UF$_6$, the 1274-keV line from ^{22}Na may become visible in UF$_6$ spectra [5]. This line is produced from the ^{19}F (α, n)

reaction and could be used to reveal the presence of HEU material hidden behind a thin layer of LEU in a UF_6 drum. The infinite thickness at 1274 keV photon is about 24 cm in solid UF_6.

The presence of lines from ^{137}Cs and [233]Pa (a daughter of [237]U) were also observed during the measurement of UF_6 product from reprocessing of spent fuel [6]. In spite of the fact that the backscattered peak of ^{137}Cs is located at 184.2 keV (figure 4), the assay results of [6] based on the analysis of the [235]U enrichment at 185.7 keV were very good.
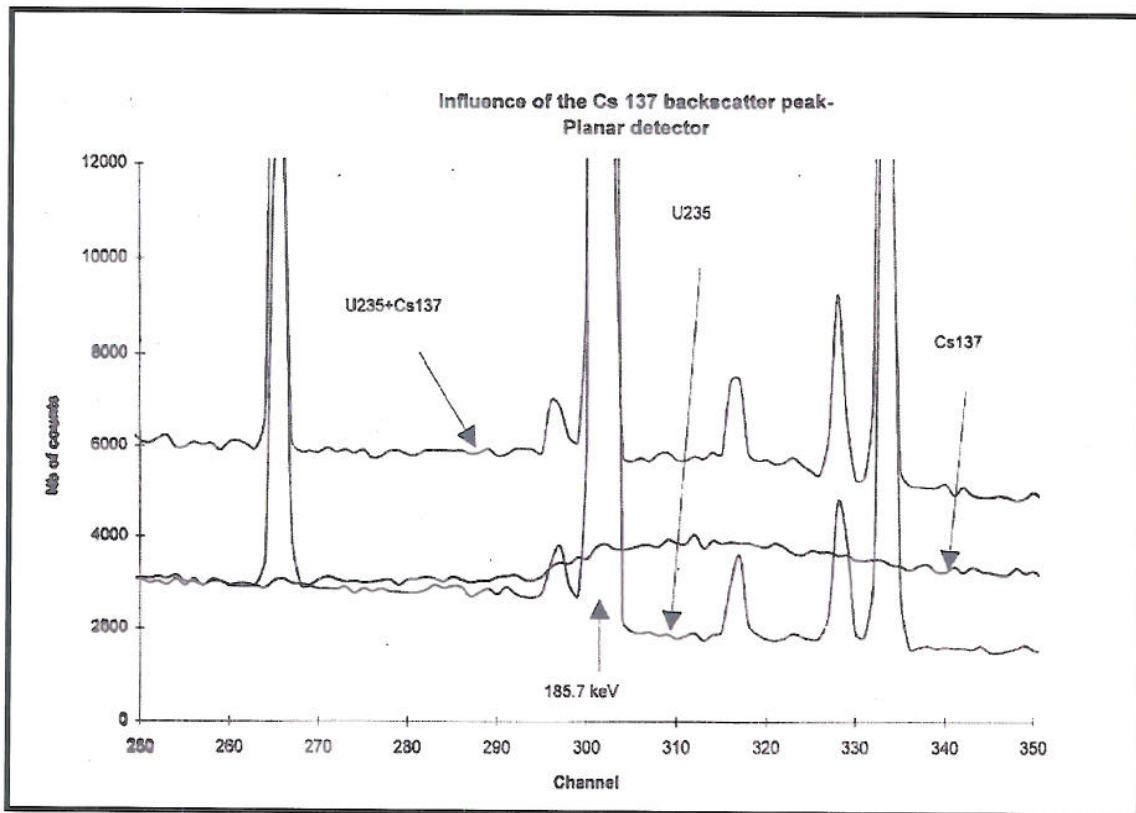
Figure 4: Influence of the ^{137}Cs peak on the U spectrum

A 3. Neutron output

In UF_6, the neutron output arises primarily from spontaneous fission of [238]U, and by [234]U alpha decay and subsequent [19]F (α, n) [22]Na reaction. Table 3 gives the relative contribution of the different U isotopes to the primary neutron production and for four typical enrichments.

Isotopes	Amount (%)	neutron source1/s/ton UF$_6$		Relative yield (%)
		spontaneous fission	UF$_6$ (α,n)	
Depleted U				
^{232}U	0	0	0	0.0
^{234}U	0.00234	0	7.85E+03	28.9
^{235}U	0.3	0	1.86E+03	6.8
^{236}U	0	0	0	0.0
^{238}U	99.6977	9.96E+03	7.53E+03	64.3
Natural U				
^{232}U	0	0	0	0.0
^{234}U	0.0056	0	1.88E+04	51.3
^{235}U	0.718	0	4.45E+02	1.2
^{236}U	0	0	0	0.0
^{238}U	99.2764	9.92E+03	7.49E+03	47.5
LEU 5%				
^{232}U	0	0	0	0.0
^{234}U	0.039	0	1.31E+05	86.9
^{235}U	5	0	3.10E+03	2.1
^{236}U	0	0	0	0.0
^{238}U	94.961	9.50E+03	7.17E+03	11.1
LEU 5% repr.				
^{232}U	7.60E-07	0	1.66E+04	3.26
^{234}U	0.133	0	4.46E+05	87.48
^{235}U	5	0	3.10E+03	0.61
^{236}U	1.55	0	2.76E+04	5.41
^{238}U	93.317	9.50E+03	7.04E+03	3.24

Table 3: relative contribution of the U isotopes to the total output neutron signal [7]

For natural uranium, the ^{234}U and ^{238}U contributions are almost equal. The ^{234}U-produced neutrons dominate the (α, n) intensity from low enriched ^{235}U. The spontaneous fission neutrons are mainly emitted by ^{238}U. ^{235}U cannot be measured directly with passive neutron measurements.

Figure 5 shows the example of a 100 group neutron spectrums for natural UF$_6$.
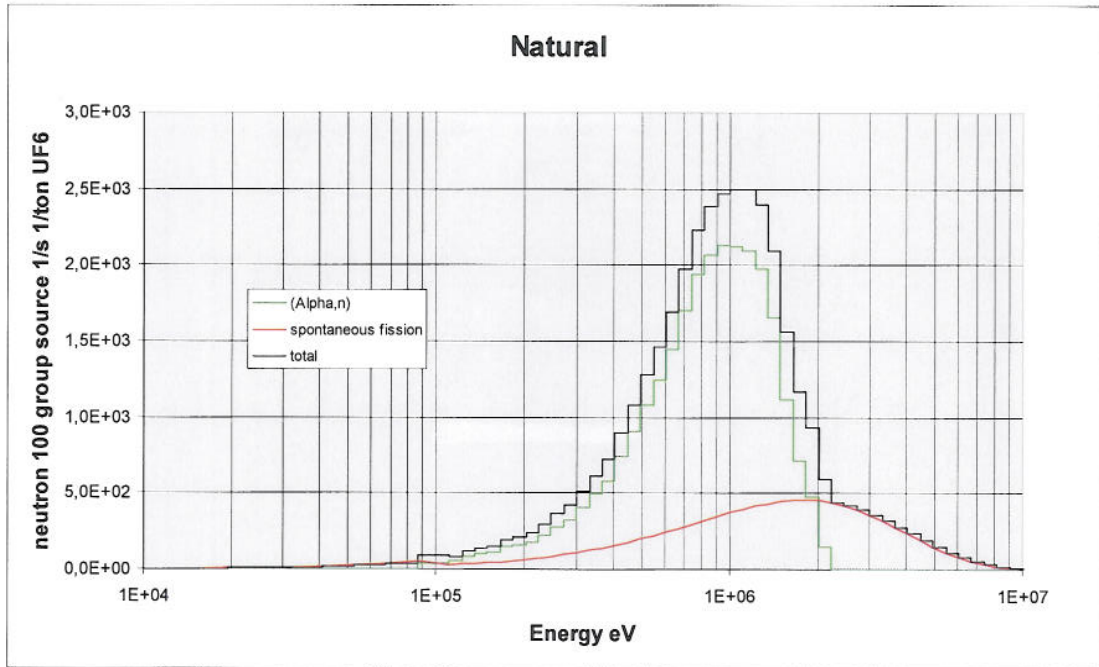
Figure 5: 100 group neutron spectrums for natural UF6 [7]

B Characteristics of the UF$_6$ cylinders

B 1. Container description

The most commonly used cylinders are the 30B (2.5 t) cylinders for low-enriched product and 48Y (12 t) cylinders for natural feed and 48G for depleted uranium storage only. Table 4 gives the characteristics of the cylinders.

Cylinder model	Nominal diameter (cm)	Nominal lengh (cm)	Nominal tare weight (kg)	Approx. Tare weight (kg)	Max enr. (weight %^{235}U)	Wall thickness (mm)	Fill limit (kg)	
							max.	min.
30B (product)	76	206	635	635	5	12.5±0.5	2.277	1.043
48Y(feed)	122	380	2359	2359	1	16±0.5	12501	9525
48G(tails)	122	370	1179	1179	1	8±0.5	12174	-

Table 4: Technical characteristics of the cylinder [8]

The cylinders are constructed of ASTM A-516 steel with a chemical composition given in table 5. Measurement performed on calibrated items lead to a sound velocity of 5910 m/s.

Element	C	Mn	Si	P	S	Ni	Cr	Mo	Cu	Al	Sn	Ti	V	Nb	N	Ce
(%)	0.15	1.21	0.21	0.011	0.003	0.014	0.18	0.007	0.012	0.035	0.001	0.019	9E-04	0.002	0.004	0.391

Table 5: Chemical composition of the steel ASTM A-516

The measurement performed in [9] showed that the 30B container thickness varies from 12.5 mm to 13.8 mm. These deviations influence strongly the enrichment determination by application of the enrichment meter principle (paragraph C1223). A variation of ±0.5 mm of the wall thickness leads to a minimum error of ± 5% of the intensity of the 185.7 keV line of ^{235}U. If there is no possibility to measure the wall thickness of the container (contact measurement) with an ultra sonic gauge, the requirement R13a of [1] cannot be fulfilled.

B 2. UF$_6$ filling profile

As it will be discussed in paragraph E 221, the neutron detector response depends strongly on the filling profile. It has to be known in order to determine the ^{235}U enrichment with passive neutron method.

UF$_6$ is characterised by a high coefficient of expansion in the liquid phase. When heated in the containment autoclaves, the transformation of UF$_6$ solid at 20 deg. to UF$_6$ liquid at 110 degrees Celsius goes with a volume increase of 53 %. Consequently, to prevent deformation and rupture of the cylinders, the maximum UF$_6$ mass does not exceed 2/3 of the maximum possible load of the cylinders.

The distribution of the material within the container depends on how it was filled, on the last operation made on it (for instance, sampling in liquid phase after homogenisation) or how long and under which conditions (temperature, sunshine) it was stored.

When it is filled in liquid phase or after sampling, UF$_6$ solidifies using all possible heat exchange surfaces. Most part of UF$_6$ remains in the lower part. However, there is a deposit of UF$_6$ of several centimetres on all the upper part (Fig 6 a).

When the container is filled by desublimation in a cylinder cooled at -25 degrees Celsius (GB2), UF$_6$ is deposited in a uniform way on all the inner surface of the cylinder (Fig 6b) and forms an annular solid ring.

When the container is filled with UF$_6$ gas at 80 degrees Celsius in a cylinder at 15 degrees Celsius, first a layer of solid UF$_6$ is deposited on the entire inner surface. Later, due to the increasing temperature of the solid UF$_6$, additional amount of UF$_6$ will condense inside the shell of solid UF$_6$, flows by gravity in the cylinder and then solidifies. Consequently, this material will fill the lower part inside the solid UF$_6$ shell (it is assumed that 75% of the gas is liquefied). As a result, we have the same filling profile than in fig 6a.
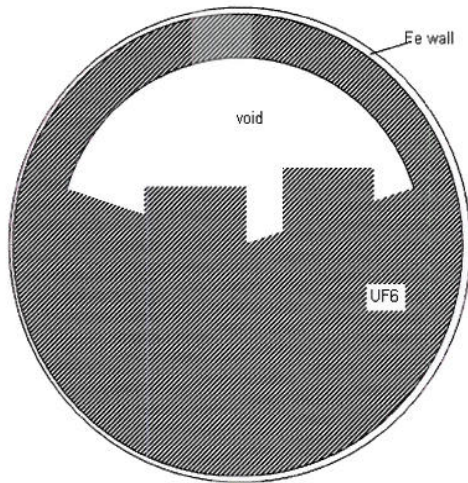
Figure 6a: Profile after filling at 80 deg C   **Figure 6b:** Profile after desublimation
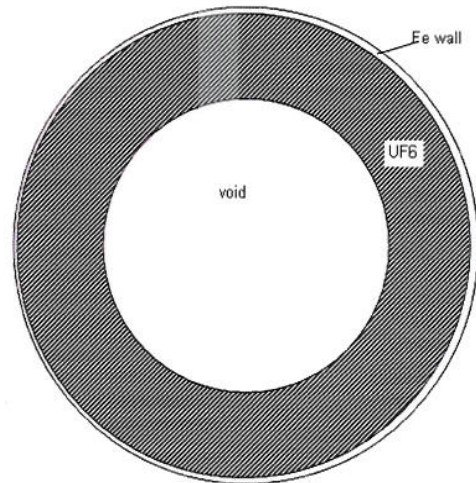
With the changes of temperatures during the day, the filling profile changes. The coating sublimes from the cylinder wall to cooler cylinder areas, thus decreasing the thickness. However, no important modification due to the daily heat cycle is expected.

Information about the effect of ambient temperature on the shape and location of the void volume in UF_6 cylinders can be found in [10].

The reference [10] mentions a study carried out at PGDP in 1971 on two 10-ton UF_6 cylinders which were filled with liquid UF_6. One of the containers was then cooled down from 93 degrees Celsius to room temperature in 15 hours whereas the other was frozen quickly in ice water at 0 degrees Celsius.

Both cylinders were then frozen and sectioned. In both cylinders the major cavities were lengthwise in the top half of the cylinder and all surfaces were covered with solid UF_6 (fig7).
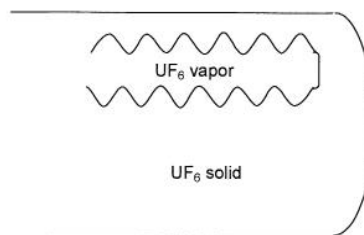
Figure 7: UF_6 filling profile

In the case of the fast cooled cylinder the cavity was much larger and the matrix was hard and dense whereas for the second case UF_6 was flaky and contained many small voids.

B 3. Chemical and radiochemical impurities

When the cylinder is emptied by gassing off the UF_6, the non-volatile daughter products of ^{238}U (^{234}Th and ^{234m}Pa) as well as uranium deposit in the form of UF_6, UO_2F_2, UF_4 and UF_5 and also volatile UF_6 remain in the "heel". On filling a freshly-emptied cylinder with UF_6, the daughter products clearly remain mainly plated on the cylinder wall. Heels in excess of 22.7 kg for 48Y or 48G and 11.3 kg for 30B require removal by cylinder cleaning. The heel is responsive for significant radiation levels observed for empty cylinders, since the non-volatile products are not self-shielded any more for an empty cylinder, the radiation dose increases by a factor of 12 for a freshly emptied 48Y cylinder and a factor of about 6 for a 30 cylinder [8].

The spatial distribution of the heel influences the amplitude and the shape of the gamma radiation background. The contribution to the spectrum of the Compton scattering of the high energy gamma rays from ^{234m}Pa as well as Bremsstrahlung production from the 2.3 MeV beta particle emitted in the decay of ^{234m}Pa are sensitive to the location of the material. In addition, since the 185-keV gamma ray used for determining the ^{235}U enrichment has a short mean free path, the deposit can mask the signal from the actual UF_6 filling.

In the measurement carried out in [9], the authors mentioned that the residual activity was often clearly defined as forming a lateral band along the length of the cylinder. This fact was confirmed by the staff of Georges Besse 1 [47]. When measuring the ^{235}U enrichment, the detector position has to be chosen in a way that the deposited does not influence the result.

As already expressed in paragraph A2, [5] [6] also mentioned the presence of ^{137}Cs and ^{133}Pa (daughter of ^{237}U) during their measurements on UF_6 cylinders.

C Review of existing NDA methods for ^{235}U enrichment and mass determination

C 1. Enrichment determination by gamma spectrometry

Introduction

Two basic NDA methods are routinely used to determine the ^{235}U enrichment. One is based on a self intrinsic calibration with unfolding of complex energy regions whereas the other makes use of the enrichment meter principle.

The choice of one or the other method is guided by the characteristics of the sample to be measure (mass of uranium material, geometry of the container, isotopic composition inducing interferences) as well as the availability of reference samples.

Each method and its and limitations are described in the next paragraphs.

C 1.1. Intrinsic calibration

The methods based on the self intrinsic calibration procedure are either based on the unfolding of the complex 80-120 keV energy region (fig 1a) or on the higher energy region 120-2600 keV.

C 1.1.1. Method based on the unfolding of the 80-120 keV region or of the 60-210 keV region

Applying an iterative procedure to separate the contributions of [235]U and [238]U in the 80-120 keV region (see, figure 2a, Paragraph A2); it is possible to determine the enrichment using an intrinsic efficiency calibration procedure. Originally mentioned in [11], this method developed and implemented in the MGAU code in 1994 [12] is widely used in the field for characterizing a wide variety of samples.

A similar approach is also used in the "URADOS" process [13], FRAM [14] and GXW [15].

MGAU

MGAU is the code which was the most intensively tested [16], [17], and [18]. It was continuously improved and has recently undergone developments [19] which would reduce the overestimation for LEU and under estimation for HEU of the previous versions [16], [18], [20] and gives a better estimation of [234]U whose 120 keV line content is now calculated using a relative efficiency curve based on the analysis of lines at 143, 163, 185.7 and 205 keV.

The authors of [19] conclude that the upgraded version would provide systematic bias close to 1% for [235]U for enrichment ranging from 0.32 to 93.2% and systematic bias close to 3% for [234]U for a concentration ranging from 0.002 to 0.98%.

FRAM

A more recently developed application of FRAM (Fixed-Energy Response-Function Analysis with Multiple Efficiency), version 4, calculates a similar efficiency curve in the 60-210 keV region.

The calculations are carried out using either a "physical-efficiency curve" taking the principal physical processes (self absorption within the sample, absorption in the sample container , absorption in interposed shielding interposed between the source and the detector and the efficiency of the detector) taking place in the sample/detector system or a "empirical efficiency model".

The existence of bias mentioned in [21] suggests that further upgrading of the code should be carried out. Up to now and compared to MGAU, FRAM-U was not tested intensively by an independent laboratory.

GXW

Based on the intrinsic calibration calculation principle, the GXW (Gamma X-ray Weighting) Analysis software also allows the determination of the [235]U enrichment as well as the U concentration for a certain type of samples and under specified conditions [15].

Measurement results tabulated in [22, 23] showed deviation up to 35% for depleted Uranium and around up to 5% for high enriched uranium.

Applicability limitations of MGAU, FRAM and GXW

MGAU, FRAM-U or GXW are based on the deconvolution of a complex region between 80 and 120 keV or 60-210 keV region, hence requiring the use of a very high resolution planar detector.

In spite of the fact that corrections for non secular equilibrium were introduced for MGAU and FRAM-U, these options were not intensively tested.

The most important factor which limits the application of these three codes is that thick shieldings interposed between the detector and the U material absorb strongly the radiation emitted in the 60-210 region used for the analysis, hence limiting the applicability to a maximum of 8 mm equivalent steel interposed shielding.

Measurements on UF_6 cylinders with 13-16 mm thick steel walls and the low-energy analysis preclude the use of these three codes.

C 1.1.2. Method based on the analysis of the 120-1200 keV region

Several attempts were made to overcome the previous limitation when measuring U in thick containers [24, 25]. These papers refer to the analysis of the 120-1200 keV region by intrinsic calibration using, the 143.8-163.3, 185.7 and 205.3 keV of [235]U and the 258.3, 766.6 and 1001 keV from [234m]Pa, with an additional gamma ray from [234]U at 120.9-keV for [24] only. Using either standard empirical relative efficiency curve or physical model for the sample detection system, these two applications were tested with various uranium enrichment standards using in particular 13 to 16 mm steel absorber and different germanium detectors.
In [24], two low enriched samples were measured for a minimum time of 30 mn and the analysis gives deviation between declared and measured below 3%.
In [25] five LEU samples were measured repeatedly 24 times for 15 mn, 30 mn or 60 mn and with 13 or 16 mm steel. For counting time of 15 mn, the average on the 24 measurements gives results deviations between measured and declared below 3%.

In spite of the good results presented in [24] [25], the tests were performed on a limited number of items, for long counting time and with detector put at the contact of the cylinder.

In case, the distance of 50 cm from the cylinder had to be respected; strong collimation would be required which would require even higher counting time to get the same good results.

However, both cases are based on gamma ray analysis below 200 keV. Since UF_6 is very absorbent the measurement results indicate only the enrichment at the drum wall.

Another important limitation is that since this method makes use of the [234m]Pa gamma lines, the secular equilibrium of [234]Th has to be reached.

C 1.2. Method based on the analysis of the 185.7 keV line of ^{235}U

The classical method used to determine the ^{235}U enrichment requires the use of reference samples and is based on the enrichment meter principle [26] applicable to infinite thick items.

This method is used routinely to determine the ^{235}U enrichment on UF_6 containers either with low resolution detector [5-6-27] or high resolution detector [9-28].

On the whole, the limitations encountered with the application of this method are defined as a function of either the performance of the used detectors (NaI, $LaBr_3$, Ge or CZT) in term of efficiency or resolution or of the algorithms used in the analysis codes (table 6).

Detector type	Ge	NaI		CZT
Code	UF6	U235	NaIGEM	
Number of calibration standards	1	2	1	1
Possibility to perform wall thickness correction	yes	no	yes	yes
taking into account of possible interference	yes	no	yes	yes
Bibliographic Reference	[5,6,9,27,28,31, 32]	[5,6]	[29]	[30]

Table 6: Applicability limitations of the enrichment meter principle as a function of the detector types

The following paragraphs present a review of different possible applications of the enrichment meter principle with the limitations of applicability for routinely used detectors. The enrichment determination with the newly developed $LaBr_3$ detector will be presented in chapter C.

C 1.2.1. Measurement of the enrichment with a NaI detector

The NaI detectors are characterized by an easy handling and high counting efficiency.

The net peak area determination is complicated as the broad full energy peak covers all the U-235 peaks from 143 keV to 205 keV. The shape of the underlying background radiation cannot be considered as a straight line. Therefore the background must be modelled within either with a fitting procedure or monitored in a adequate region of interest at a higher energy in the spectrum.
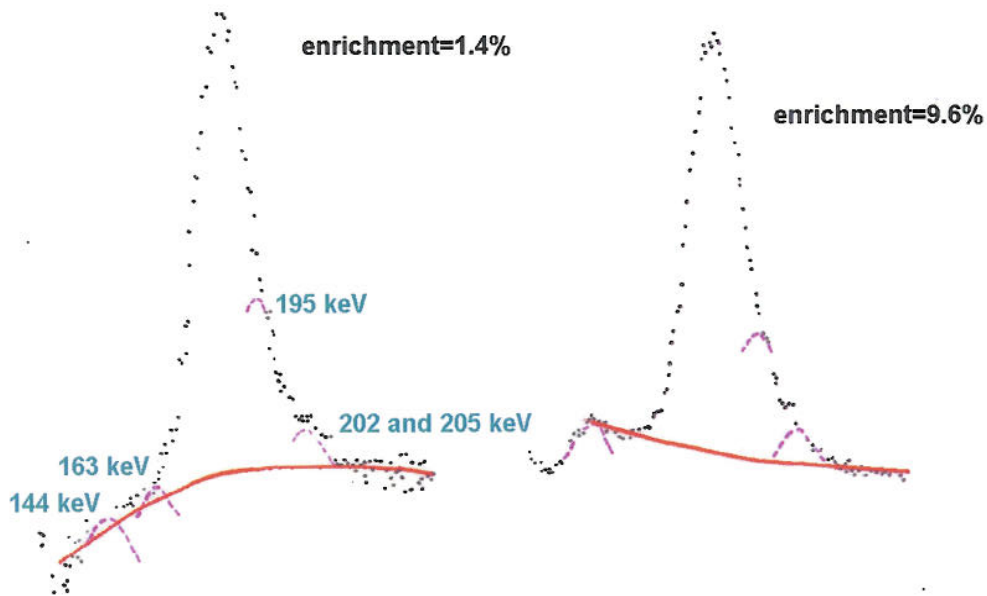
Figure 8: Background below the 185.7 keV line for two different enrichments

C 1.2.1.1. Two window counting technique

When the background is monitored with an adequate region of interest, the technique is called "two window counting ". The enrichment is expressed with the following expression:

$$E= A*ROI_1-B*ROI_2$$

where:

- A and B are the two calibration constants ,
- ROI_1 , a window bracketing the 185 keV peak,
- ROI_2, a second window set just above the peak to evaluate the background.

The "two window counting technique" cannot be applied when:

- the shape of the background is time dependent or change because of plated ^{234m}Pa heel mask the signal from the actual UF_6 filling,
- the container wall thickness for calibration standard and sample to be measured have a difference of more than 2 mm equivalent steel,
- gamma peak interference are expected,

23

Wall thickness correction:

The wall thickness correction factor K_{wtc} which accounts for difference in wall thickness between the calibration standard and the sample to be measured cannot be calculated easily because ROI_1 and ROI_2 are influenced in different proportion by:

- the Compton background of the lines at 766 and 1001 keV of [234m]Pa,
- the bremstrahlung production from the 2.3 MeV beta particle emitted copiously in the [234m]Pa decay,
- the scattered radiation of these same rays in the interposed shielding and,
- the scattered radiation in the source itself.

Even if this correction is implemented in IMCA [33] used by IAEA, the correction works only for small deviation compared to the calibration (less than 2 mm equivalent steel).
To avoid the misuse of this correction factor, this correction was not implemented in code such as U235 software [34] used with the MCA-166.

This wall thickness correction can be properly calculated when calculating the net peak area background with a fitting procedure with the NaIGEM code [29]. This code integrates a wall thickness correction which works properly for a for a Collimator Diameter /Collimator Height ratio below 1.7 [35]. A more extended calculation for a non parallel beam was proposed in [36].

Gamma peak interference:

Interference occurs when gamma lines other than from [235]U are so close to 186 keV that they cannot be resolved by the detector. The drawback of a NaI detector is obvious.
In order to estimate the resulting measurement inaccuracy, the count rate of interfering gamma lines of [232]U, [234]U, [238] U can be figured out from table 7a to 7d. These tables give gamma lines of interest, the number of photons/s and initial gram for each isotope and T represents the time after chemical separation. Table 8 gives the relative contribution of the isotopes ([232]U, [234]U, [238] U) to the 185 keV line taking into account a resolution of 30 keV for an energy E=186 keV.

[232]U		Photons/s per initial g of [232]U		
Energy(keV)		T=0	T=1y	T=10y
164	[212]Bi	0	$1.1\ 10^7$	$3.2\ 10^7$
166.4	[228]Th	0	$2.3\ 10^8$	$6.9\ 10^8$
176.7	[212]Pb	0	1.2108	$3.6\ 10^8$
182.2	[228]Th	0	$1.3\ 10^4$	$3.7\ 10^4$
205.9	[228]Th	0	$4.4\ 10^7$	$1.3\ 10^8$
238.8	[212]Pb	0	$1\ 10^{11}$	$3.1\ 10^{11}$
270.2	[232]U	2.3 17	$2.3\ 10^7$	$2.1\ 10^7$

Table 7a: Photons/s per initial gram of [232]U
(T - time after chemical separation)

^{234}U		Photons/s per initial g of ^{234}U		
Energy(keV)		T=0	T=1y	T=10y
185.8	^{230}Th	0.2	0.9	1.8
186.2	^{226}Ra	0.02	0.4	1.6
241.9	^{214}Pb	0.04	0.8	3.3

Table 7b: Photons/s per initial gram of ^{234}U

^{235}U		Photons/s per initial g of ^{235}U	
Energy(keV)		T=1y	T=10y
163.1	^{231}Th	$1.3 \ 10^2$	
163.4	^{235}U	$4.0 \ 10^3$	
174.2	^{231}Th	$1.5 \ 10^1$	
182.1	^{235}U	$3.4 \ 10^2$	
183.5	^{231}Th	$2.8 \ 10^1$	
185.7	^{235}U	$4.6 \ 10^4$	
194.9	^{235}U	$5.0 \ 10^2$	
198.9	^{235}U	$3.2 \ 10^1$	
202.1	^{235}U	$8.5 \ 10^2$	
205.3	^{235}U	$4.0 \ 10^3$	

Table 7c: Photons/s per initial gram of ^{235}U

^{238}U		Photons/s per initial g of ^{238}U
Energy(keV)		T=1y
159.1	^{234}Pa	0.1
170.7	^{234}Pa	0.08
174.6	^{234}Pa	0.03
184.7	^{234m}Pa	0.15
186	^{234}Pa	0.32
193.4	^{234m}Pa	0.06
193.6	^{234m}Pa	0.1
196.4	^{234}Pa	0.01
199.9	^{234m}Pa	0.05
200.6	^{234}Pa	0.18
203	^{234}Pa	0.19

Table 7d: Photons/s per initial gram of ^{238}U

Interference from the decay of ^{238}U

Natural Uranium contains 99.28 % of ^{238}U ($T_{1/2}$= 4.468.10^9 years) which decays into ^{234}Th ($T_{1/2}$=24.1d), which in turn decays by beta decay to ^{234m}Pa ($T_{1/2}$= 1.17 mn) and ^{234}Pa $T_{1/2}$=6.7h). These two ^{238}U daughters are always present in uranium samples. Table 7d shows the gamma lines of uranium in both energy and background window for secular equilibrium. There are two sorts of impact on the measurement precision:

- the sample to be verified is not yet in secular equilibrium after reprocessing and hence contains less protactinium than the calibration standard,

- additional photons are emitted from the heel so that the sample contains more protactinium than the calibration standard.

There are two interfering lines very close to the 185.7 keV line (table 7d) that cannot be resolved even with a Germanium detector:

- at 184.7 keV emitted from ^{234m}Pa, 0.15 photons/s /per initial gram of ^{238}U,
- at 186.0 keV emitted from 0.32 photons/s/ per initial gram of ^{234}Pa,

Table 6 shows for several enrichments the contribution to the 185.7 keV line of all the lines of ^{234}Pa and ^{234m}Pa interfering with this peak when the secular equilibrium is reached.

Detector type	Enrichment (%)	Contribution of ^{238}U and decay products to the 185.7 keV line (%)
Germanium	0.3	0.34
	0.7	0.14
	1	0.1
	5	0.02
Nal	0.3	0.84
	0.7	0.24
	1	0.25
	5	0.05

Table 8: Contribution of the ^{238}U and decay products to the 185.7 keV line

One can see that for depleted uranium, the contribution of ^{238}U decay product is around 0.8%.

Uranium daughters from the heel however can bias the measurement to a much greater extent [9].

Interference from the decay of ^{232}U

Significant interference is to be expected from reprocessed fuel in particular from the isotope ^{232}U.
^{232}U has a half life of 72 years. It grows in after chemical separation from the decay of one of the uranium isotopes that are produced through nuclear reaction. It reaches a flat maximum within 10 years. As an example, its concentration in originally 3.2 % enriched LWR fuel of a burn-up of 33000 MWD/t, 3650 days after discharge from the reactor, is 8.2×10^{-4} g/ton of fuel charged to the reactor compared to $7.5.10^{3}$ g/t of ^{235}U. The ^{232}U to ^{235}U ratio is hence 1.1×10^{-7}.

Looking at table 5a, there is an emission of 3.7×10^4 photon/s/g and initial gram at 182.2 keV which would interfere with the 186 keV line of ^{235}U of the same order of magnitude (4.6×10^4 photons/s/g). However, the contribution of this line remains negligible (even for a germanium detector). For instance, the contribution of ^{232}U decay lines to the 185.7 keV line is 0.001 % for a 5% re enriched reprocessed uranium.

A considerable bias, however, has to be expected from measurements with NaI where several strong lines, esp. the 238.6 keV line of ^{212}Pb invade the background window. A background estimation based on a region which would not contain gamma line of ^{232}U should be chosen in a way that it is not anymore influence by the ^{232}U separation time.

Conclusion:

The use of the NaI detector is made difficult due to:

- the presence of ^{234}Pa in the heel,
- the potential presence of ^{232}U and decay with interfering lines in both energy- and background window,
- the sensitivity of the enrichment determination as a function of the variation in wall thickness (0.05 cm variation in wall reflects a relative change of 5% in the measured enrichment).

C 1.2.1.2. Fitting technique - NaIGEM

The limitations imposed by the use of the two window counting can be overcome by fitting the background below the 185.7 keV line. The NaIGEM software [29] applies the enrichment meter principle but in contrary to the two window counting technique, the 185.7 keV net peak area is calculated by a non linear least square fitting procedure.

The enrichment is expressed as:

$$E = C * K_m * K_{wtc} * \text{ net peak area of 185.7 keV line}$$

where C is the calibration constant, K_m and K_{wtc} the matrix and wall thickness correction factor respectively. These two parameters correct for container-standard mismatches (the sample matrix, the thickness and type of attenuating material between the source and the detector).

The code can be applied for collimator diameter/thickness ratio lower than 1.7. However, further developments [36] may extend its use to larger diameter/thickness ratios. Tested on the PERLA standards, the code gives satisfying results with interposed shields up to 17 mm steel [35]. However, the test of the code with reprocessed uranium is very limited.

C 1.2.2. Measurement of the enrichment with semiconductor detectors

C 1.2.2.1. Germanium detector

High Resolution germanium detectors are required when two or more gamma lines are likely to overlap e.g. for measurements of reprocessed fuel where gamma emission from isotopes other than ^{235}U can be expected. The photo peak of the 185.7 keV is narrow enough to allow for background subtraction by a straight line. The germanium detectors are routinely used to measure the UF_6 containers [28, 27, 32, 9, 31, 37].

The wall thickness correction factor calculation can be evaluated on the basis of the simple assumption of a quasi parallel beam. In the case of large collimator aperture, more sophisticated correction factor have to be calculated which are not taken into account in commercialised codes.

Table 9 summarizes the measurement conditions of the different measurement campaigns cited from literature.

Reference	Year/Author	Detector type	Collimator	Distance detector- cylinder	Nb of measured cylinder cylinders, cylinder type	Counting time (s)	Accuracy
[28]	**1998** Hagenauer		Lead plug diameter=1.3cm lateral collimator	contact	700, 5-,8-,12-, inches diameter containers	300	?
[31]	**2007** Montgomery	LEGe, 500mm^2 25.2mm diameter*15mm thickness	"highly collimated"	contact	1236, 30B 71, 48Y	300	sytematic uncertainty:1.6% for 30B and 48Y random uncertainty: 7.7% for 48Y and 4% for 30B
[9]	**1979** Shaw	Princeton gamma- tech intrinsic Ge detector	lateral shielding 5cm wall detector back shielding	contact	130, 30B	300	coefficient of variation around 2% per batch
[37]	**1997** Berndt	Ge-planar GI-1020-R	diameter=36 mm h=20mm	contact	30B and 48Y	300 to 1000	total uncertainty:20% for depleted and 2% for 3.7% enriched uranium
[32]	**1979** E.Dermendjiev	Ge, 56 cc	?	contact	22, 30B	300 to 600	total uncertainty: 8%

Table 9: measurement conditions and resulting accuracy for measurement campaigns described in the literature

For all the series of measurements, the detector was placed as near as possible to the cylinder and very often at a point about half a cylinder diameter above the ground.

In [31], the detector was in UF_6 cylinder storage area where adjacent containers were placed and cylinders stacked in some cases.

It is worth mentioning that:

-for ref [28] [31] [37], the wall thickness was determined at the position of the gamma measurement to insure that non-homogeneous cylinder wall thickness would affect the quality of the measurement. In some cases, a wall thickness corresponding to 13 mm was taken as a mean value [9].

-ref [9] showed that there was significant interference from the gamma emission of adjacent cylinders and that the detector was vulnerable to interference from cylinders sited directly behind the cryostat and that the ratio signal/background was improved by using a 5 cm lead shield collimator which held the detector face for a NaI detector.

C 1.2.2.2. Large CZT detector

The capabilities of a portable, ambient temperature CZT/1500 for uranium enrichment determination were also investigated in a laboratory study. Its resolution (13 keV at 185.7 keV) is good enough to avoid the complication due to interference and to allow an easy subtraction of the background by fitting.

Its absolute full energy peak efficiency at 185.7 keV is slightly better than that of a planar germanium detector with 1.6 cm diameter and 1 cm thickness [30].

In this study, the detector was placed on contact with the samples. Steel plates were placed between the detector and the uranium standard to mimic the cylinder wall. For counting time of 300 s, the measurement of depleted uranium (enr = 0.3166%) and of natural uranium (enr= 0.7119%) behind 16.8 mm steel gave respectively (0.1644± 0.0413) and (0.7085± 0.1086).

C 1.2.2.3. Main parameters affecting the uncertainties associated to the determination of the enrichment with a semi conductor detector

The enrichment meter principle is based on the comparison of the 185.7 keV peak net area of an unknown sample to a calibration standard relying on the proportionality of count rate and enrichment. It is expressed as [36]:

$$\frac{E_s}{E_c} = \frac{CR_{186,s}}{CR_{186,c}} * f_m * f_{wtc}$$

Where:

s is the index   for the sample,

c is the index   for the calibration standard,

E ^{235}U enrichment,

CR_{186} 186 keV peak net area counts per time unit,

f_m matrix correction factor,

f_{wtc} wall thickness correction factor.

The parameter f_{wtc} corrects for the different materials and wall thicknesses of sample and calibration standard. It is equal to

$$f_{wtc} = \frac{\exp(-\mu_c * \rho_c * K_{wtc,c} * x_c)}{\exp(-\mu_s * \rho_s * K_{wtc,s} * x_s)}$$

Where

      S   the index for the sample,

      c   the index for the calibration standard,

      μ mass attenuation coefficient of the shielding between source and detector,

      ρ density of the shielding material,

      x   thickness of the shielding,

      K_{wtc} geometric correction factor for a non-parallel beam crossing the shielding

The geometrical correction factor K_{wtc} takes into account the increase of the attenuation for a non parallel beam [36].

The parameter f_m is equal to

$$f_m = \frac{[U]_c}{[U]_s} * \frac{\mu_s}{\mu_c}$$

Where

      S   the index for the sample,

      c   the index for the calibration standard,

      μ mass attenuation coefficient of the matrix

      [U]   U concentration factor

The variance $V(E_s)$ of the calculated enrichment derivates from the elementary uncertainty propagation law:

$$\frac{V(E_s)}{E_s} = \frac{V(E_c)}{E_c^2} + \frac{V(f_m)}{f_m^2} + \frac{V(f_{wtc})}{f_{wtc}^2} + \frac{V(CR_{185,c})}{CR_{185,s}^2} + \frac{V(CR_{185,s})}{CR_{185,c}^2}$$

In this expression, the predominant contribution comes from the count rates in the 185.7 keV line for the sample and calibration and the wall thickness correction.

The accuracy of the count rate in the 185.7 keV line is influenced by the ratio peak/background which can be optimized by an appropriate collimation system. It was found the that the photo peak to background ratio could

be improved marginally by using a collimator that holds the detector face some 5 cm away from the cylinder surface [32].

The sensibility of the enrichment determination accuracy as a function of the wall thickness correction factor uncertainty can be illustrated with numerical application in typical cases.

The uncertainty of the wall thickness correction factor f_{wtc} (2) is express by:

$$\left(\frac{\Delta f_{wtc}}{f_{wtc}}\right)^2 = \left(\mu_c * \rho_c * K_{wtc\,c} * x_c\right)^2 * \left[\left(\frac{\Delta \mu_c}{\mu_c}\right)^2 + \left(\frac{\Delta \rho_c}{\rho_c}\right)^2 + \left(\frac{\Delta K_{wtc\,c}}{K_{wtc\,c}}\right)^2 + \left(\frac{\Delta x_c}{x_c}\right)^2\right] +$$

$$+ \left(\mu_s * \rho_s * K_{wtc\,s} * x_s\right)^2 * \left[\left(\frac{\Delta \mu_s}{\mu_s}\right)^2 + \left(\frac{\Delta \rho_s}{\rho_s}\right)^2 + \left(\frac{\Delta K_{wtc\,s}}{K_{wtc\,s}}\right)^2 + \left(\frac{\Delta x_s}{x_s}\right)^2\right]$$

In the field, the measurements are preceded by a wall thickness measurement by means of an ultrasonic thickness gauge calibrated with a certified test block made of the same steel material. The detector is placed as near as possible to the cylinders and the thickness is determined at the position of the measurement.

Reference [9] mentioned that the 30B container thicknesses varies from 12.5 mm to 13.8 mm for the 30B containers whereas the wall thickness variations measured in [38] are given in the table 10:

48Y				30B			
end surface		side surface		end surface		side surface	
min	max	min	max	min	max	min	max
16.7	17.21	16.18	16.53	13.7	14	12.77	13.38

Table 10: Thickness variation on UF$_6$ containers (mm)

The uncertainty $\Delta f_{wtc}/f_{wtc}$ is equal to **5.5%** for x_c= (16.0 ± 0.1) mm and x_s= (17.0 ± 0.5) mm for a 48Y container and to **5.7%** for x_c= (13.0 ± 0.01) mm and x_s= (13.5 ± 0.5) mm for a 30B container.

These numerical values show that a typical wall thickness variation from nominal value easily leads to an enrichment error of 6%.

Conclusion:

Gamma measurements are surface measurements which allow determining the ^{235}U enrichment only for the maximum 2 cm thick UF$_6$ layer in contact with the steel container. The bulk of the drum contents remains invisible[1].

The only applicable method to measure the ^{235}U enrichment by gamma spectrometry is to use the enrichment meter principle of the analysis of the 185.7 keV gamma rays of ^{235}U. The accuracy on the result depends strongly on the quality of the wall thickness correction. Since in the requested set-up the wall thickness can not be measured with an ultra sonic gauge, the variation of this parameter will cause systematic errors in the order of 6% and hence the requested systematic error of 2 % [1, R13a] cannot be achieved.

The germanium detector can be used (within the above mentioned limits). For all the cited references, the measurements were performed with the detector very close to the cylinders whereas for this study, the distance detector to cylinders distance must at least be equal to 50 cm to insure safe motion of the cylinders. Under these conditions the achievable count rate is limited (also after optimisation of the collimation) and leads to large random errors above the requested limits in [1] .(see below chapter E1).

The sodium iodine detector suffers from potential presence of protactinium deposit in the inner wall of the cylinder and possible gamma ray interference.

The low efficiency of the CZT detectors limits their use for this application.

C 2. UF$_6$ mass and ^{235}U enrichment determination with passive and active neutron assay

Introduction

Passive and active neutron measurement techniques have been used to determine both the ^{235}U enrichment and UF$_6$ mass [5, 6, 39]. The purpose of the next section is to describe the different assay measurements referred in the literature for both passive and active techniques and to see how the results could be used in our study.

C 2.1. Passive neutron assay

The passive neutron detection consists in measuring the fast neutron flux emerging from a UF$_6$ cylinder. The primary flux is due to F(α, n) reactions induced by the ^{234}U alpha activity. If a constant ^{235}U/^{234}U ratio can be assumed, the fast neutron flux is then proportional to ^{235}U.

---

[1] A 0.5 mm thick layer of deposits of an earlier filling represents 4% of the UF$_6$ mass the gamma detector "sees". The enrichment value of this old material contributes with a weight factor of 0.04 to the measurement result, whereas the enrichment value of the interesting new material with a factor 0.96. A 0.5 mm deposit of 2% enriched U will cause a relative enrichment error of 3% in case the bulk of the drum has 5% enrichment.
In [6] larger errors are estimated. But it is only an estimate without additional experimental input. The authors do not assume that the observed outliers of their measurement results are caused by internal deposits.

The total neutron source term from a mass of UF_6 can be written as:

$$Q = M_u \cdot (3230000 \cdot f_{32} + 496 \cdot f_{34} + 0.0917 \cdot f_{35} + 2.64 \cdot f_{36} + (0.0112 + SF_{38}) \cdot f_{38}) \quad [7],$$

where Q is the neutron source strength in n/sec, M_u is the uranium mass in g, f is the fractional isotopic composition of the subscripted isotope and SF_{38} spontaneous fission coefficient of ^{238}U.

If the terms with f_{32}, f_{35} and f_{36} can be neglected, the previous expression becomes:

$$Q = M_u \cdot (496 \cdot f_{34} + ((0.0112 + SF_{38}) \cdot f_{38})$$

If the ratio $^{234}U/^{235}U$ is known and constant, the neutron source strength can be written as:

$$Q = M_u \cdot (a + b \cdot f_{35})$$

Several experiments [5, 6] were carried out to define the relationship between the neutron detector response, the ^{235}U enrichment and the total UF_6 mass. Table 11a summarizes the different experimental parameters and conclusions of these two papers.

Reference /year	Type and numbers of measured containers	Detector	Distance container-detector	Background (counts/mn)	Count rate (counts/mn)	Conclusions
[6] 1974	30B 123	SNAP* back angle shielding factor 4.2 and 2.3 for background neutron from ^{238}Pu-Li and ^{252}Cf resp. abs. efficiency:8*10-5 at 1m for the ^{238}PuLi source	contact 4 and 8 o'clock toward the centre of the cylinder	<350	4950 for 3% enriched material	neutron count rate= a+b* ^{235}U enr with a and b function of M_{UF6} For a fixed ^{235}U enrichment:leakage fraction varies from 0.93 to 0.82 as the UF_6 weight increases from 2000 to 5000lb For a fixed UF_6 mass, leakage fraction varies from 0.80 to 0.84 as the enrichment varies from 1 % to 4% mass determination was accurate within about ± 15% even with lighter cylinders (1140 to 3000 lb). - the method presented a standard deviation of only 6.5% for the distribution of the parameter (E measured- E declared) when applied to the measurement of 110 type 30B cylinders with enrichment >1%.
[5] 1981	30A 14 cylinders full or partially full (1000 to 2230kg) ^{234}U varies from 0.01% to 0.03%	2 ^{4}He tubes with moderator 18-atm fill pressure	contact midpoint of the cylinder length			neutron count rate= a+b* ^{235}U enr with a and b function of M_{UF6}
	30A 16 fixed $^{234}U/^{235}U$ ratio	SNAP* back angle shielding factor 4.2 for background neutron from ^{238}PuLi abs. efficiency: 5.8*10^{-5} at 1m for the same source	contact	50 to 100	3200cts/mn for 3.1% enr	neutron count rate= a+b* ^{235}U enr with a and b function of M_{UF6}

Table 11a: Passive neutron measurement

The results lead to the conclusion that there is a linear relation ship between the detector response and the enrichment for a given UF_6 mass for an enrichment ranging from depleted to 5%.

In addition, the variations in the neutron leakage (fraction of the source neutron that escape from the cylinder) per source neutron caused by larges changes in enrichment and cylinders loadings were small. If the neutron leakage would vary dramatically with the weight or the enrichment, it meant that only a fraction of the load would contribute to the total number of counts.

In conclusion, the passive neutron counting is not directly sensitive to ^{235}U content, but if the ratio ^{234}U/^{235}U is known, the UF$_6$ mass and isotopic composition of 30B cylinders can be checked. However, it is necessary to supplement these experimental results with MCNP calculations to confirm the relationship between the neutron output and the UF$_6$ weight or the ^{235}U enrichment.

However, a falsification of the ^{235}U enrichment declaration which can not be detected by gamma spectrometry could lead to the expected neutron count rate (i.e. according to the declaration) when compensating the missing neutrons with HEU material hidden in the cylinder.

C 2.2. Active neutron interrogation

The active measurement technique is a direct measurement of the ^{235}U enrichment and in contrary to the passive measurement, there is no need to know the ^{234}U/^{235}U ratio. Table 11b summarizes the experiments performed in the 70's with techniques based on thermal neutron induced fission of ^{235}U in UF$_6$ cylinders. Figure 9a and 9b show the device used in [6] and the measurement geometry.

Reference /year	Type and numbers of measured containers	Detector	Source	Distance container-detector	Count rate (counts/mn)	Conclusions
[6] 1974	30B 38 up to 4% enrichment	4 ^{4}He tubes with moderator 18-atm fill pressure Cadmium foil to remove interrogation neutron	moderated Am-Li (5.10^{5}n/s)	contact	3500 for 1% enrichement	up to 3 % neutron count rate=(a+b* ^{235}U enr) up to 4% neutron count rate≠(a+b* ^{235}U enr)
[5] 1981	30A 14 cylinders full or partially full ^{235}U varies from 1.35% to 3.93%	2 ^{4}He tubes with moderator 18-atm fill pressure	moderated Am-Li (5.10^{5}n/s) or ^{238}Pu-Li (1.5.10^{5}n/s)	contact	3000 for 2% enriched	linear or quadratic fit of the function: neutron count rate=(a+b* ^{235}U enr)
[39] 1973	30B and 48Y 21 fixed ^{234}U/^{235}U ratio	2 ^{4}He tubes with moderator 18-atm fill pressure	Am-Li (5.10^{5}n/s) or ^{238}Pu-Li (1.5.10^{5}n/s)	contact	3000 for 2% enriched U	neutron count rate=(a+b* ^{235}U enr) up to 3% enrichment Accuracy ± 5% for a 2 mn counting time

Table 11b: Active neutron measurements

The mean-free-path for thermal neutrons in solid UF$_6$ is a strong function of ^{235}U enrichment varying from 24 cm for 0.3% to 4 cm for 4%. This leads to a correspondingly strong dependence of the detected induced-fission on fast neutron flux on ^{235}U enrichment.

Table 11b shows that, up to 3% the net count rate is a linear function of the enrichment for the three experiments whereas on the 0.3 -4% enrichment range, results of [6] show a non linear behaviour which was then confirmed with MCNP calculations.

34
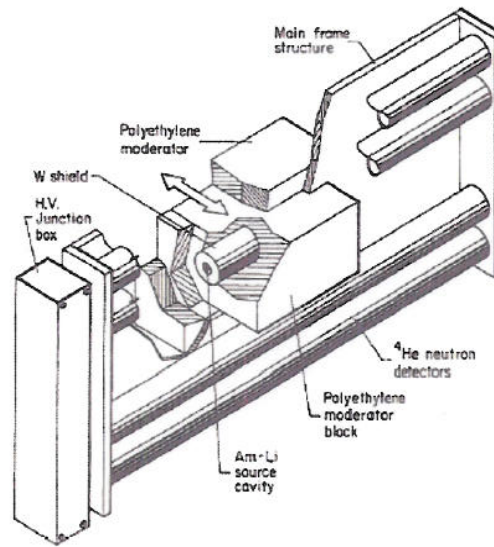
Figure 9a: Schematic drawing of the measurement device [6]

Figure 9b: Measurement geometry with active device [5]

Conclusion

Contrary to the gamma spectrometric measurements, passive and active neutron based techniques are not sensitive to deposits of protactinium, to the container wall thickness variation and to the presence of potential interference.

Passive neutron measurements require the knowledge of the $^{234}U/^{235}U$ ratio. References [5, 6] showed that adequate calibrations allowed the determination of the ^{235}U enrichment as well as the total UF_6 mass.

The small variation of neutron leakage factor as a function of the enrichment or as a function of the UF_6 mass of [6] have to be confirmed with MCNP simulations to see whether all the source volume elements contribute significantly to the total signal. The work will be described in chapter E.

The active measurement technique is a direct measurement of the ^{235}U enrichment and in contrary to the passive measurement, it does not require the knowledge of the ^{234}U/^{235}U ratio. It makes use of special geometry conditions (source and detector in contact with the container) and cannot be easily applied if the source and the detector have to be placed at 50 cm distance from the drum.

D Techniques based on the analysis of delayed neutrons and delayed photons

Introduction

Delayed neutrons and β-delayed gamma rays emitted by uranium fission products have been the object of recent investigations, especially for applications such as systems for border security monitoring or for radioactive waste management. For this purpose highly sensitivity methods are required. All these studies require the use of heavy installations (accelerators and reactors) serving as pulsed neutron or high-energy photon interrogation sources and are performed on small quantity of fissile material and none of these studies was performed on UF$_6$ transportation containers.

However, since these techniques appear as a powerful tool for determining the U enrichment/U mass in cases where traditional gamma technique cannot be applied and since they show some promising trends, the chapter below summarized some of the experiments carried out with the delayed neutrons and delayed photons.

D 1. Determination of the ^{235}U enrichment and ^{235}U mass of bulk uranium samples using delayed neutrons

The determination of the ^{235}U enrichment/^{235}U mass of small samples was investigated in [40] and [41] based on the analysis of U fission fragments decay with the emission of delayed neutrons after irradiation with neutrons.
The output of delayed neutron is small compared to that of the prompt neutron. However, the disturbing influence of the neutron background from floor and nearby objects is reduced when using a pulsed neutron source instead of an Am-Li source, hence a higher sensitivity of the method can be achieved.
These delayed neutron emitters can be categorised into 6 groups with half-lives ranging from approximately 0.2 to 55 s [42] and the total neutron count rate of each fission system is a linear summation of these six groups [43].

D 1.1. Interrogation with a 14 MeV pulse generator [40]

In[40], a series of interrogations was performed with a 14-MeV pulse generator on bulk samples shielded by lead and using a polyethylene moderated ^{3}He based neutron detection system equipped with 48 tubes (2.54 cm diameter by 100 cm length filled to a gas pressure of 0.2MPa).
The samples had a maximum weight of 1 kg and an enrichment ranging from depleted to 91%. They were irradiated for 100 s to achieve an "intrinsic steady-state". Then, the active source was switched off and the neutron response was recorded for 400 s. The temporal die away tail which is the sum of six decaying

exponentials was then fitted and the enrichment was determined from the best fit of the data. Using a six group fast fission delayed neutron precursor model, the expression of the enrichment related to the actively induced delayed neutron driven neutron response for small fissile sample irradiated was calculated. The results showed some promising trends and confirm the applicability of the method principle.

D 1.2. Interrogation with a pulsed neutron beam produced by a LINAC [41]

In [42], the neutron interrogation source was produced by the bremsstrahlung from a 4 MeV LINAC coupled first to an electron-gamma Pt converter and then to a gamma neutron heavy water converter. The neutron energy was 1.77 MeV at 4 MeV electron energy. The total counts of delayed neutrons was studied as a function of the enrichment (0.28% to 2.7%) , ^{235}U mass and total U content for samples with a total mass of around 400 g. The conclusions of the work were that:

-a linear relationship was found between the delayed neutron signal and the enrichment and the total amount of uranium,
- a sensitivity limit 0.5 g ^{235}U could be achieved in a 20 s measurement time.
Both results of [40] and [41] show that the analysis of delayed neutron is a promising technique with a low sensitivity suitable to the detection of smuggled nuclear material.

D 2. Determination of the ^{235}U mass of bulk uranium samples based on the analysis of delayed photons

D 2.1. Beta-delayed gamma above 3 MeV after irradiation with a thermal neutron flux [44]

The beta-delayed gamma rays have yields that are roughly an order of magnitude larger than the corresponding beta-delayed neutron intensities from the thermal fission of ^{235}U.

In [44] ,small quantities of Pu and other typical materials representative of cargo loadings (wood, polyethylene, aluminium, sandstone and steel) were irradiated by a **thermal neutron flux** ($1.5*10^6$cm^{-2}s^{-1}) produced by bombarding a Be target with deuterons from a Cyclotron and moderating with a 15 cm cube of steel surrounded by up to 45 cm of polyethylene. The results showed that the irradiation of steel target and other loading material produces gamma lines below 3 MeV, whereas the intense gamma rays at energies above 3 MeV are unique signatures of ^{235}U and ^{239}Pu.
By integrating the total number of events in a wide energy range (3-4 MeV and 4-8 MeV), regardless of whether the events represent full-or partial-energy depositions, it was possible in reasonable time to identify the ^{239}Pu sphere in a cargo following an irradiation of 30s.
The infinite thickness for a photon of 3 MeV in UF$_6$ material with a density of 5g/cm^3 is about 32 cm. The quantification of this high energy line could be of high interest for quantifying the UF$_6$ total mass in the transfer containers.

D 2.2. Beta-delayed gamma radiation emitted after photo fission [45]

Similar analysis of beta-delayed gamma lines were performed on nuclear waste packages using **photo fission**. Using a high energy photon beam produced by a LINAC coupled to a tungsten conversion target, small U samples were bombarded. At first, the production rate of short lived fission products was investigated.

The resulting gamma spectra were then analysed and a calibration curve giving the relationship between the weight percentage of ^{235}U from 0.7% to 85% and the ratio 974 keV ($^{132}Sb/^{132m}Sb$)/1031 keV (^{89}Rb) was calculated based on the assumption that the efficiency of the detector is the same for these two energies and for a given irradiation time and cooling time.

Compared to the experiments carried out in [44], the lines of interest are 1 MeV for which the infinite thickness is around 16 cm in UF_6 with density of 5.1g /cm^3. This would not allow a confirmation of the enrichment in the inner part of 48Y containers.

In complement to this study, it should be noted that recently efforts were made to study the ideal photon source for active interrogation of fissile material [46]. In this paper, the authors have investigated the use of low-energy proton induced nuclear reactions to generate monochromatic, MeV-energy gamma rays. The delayed gamma radiation resulting from the photo fission in uranium was studied with 12 MeV and 6 MeV photon beam produced by the nuclear resonances at 163 keV for the $^{11}B(p, \gamma)^{12}C$ reaction and at 340 keV for the $^{19}F(p, \alpha\gamma)$ ^{16}O reaction.

Conclusion

The analysis of delayed neutron/delayed gamma represents promising tools for determining the ^{235}U enrichment and U mass.

Proof of principle measurements were performed in the pre cited papers on small samples for short counting time. The used method demonstrated a high sensitivity well adapted to the detection of smuggled nuclear material.

In all experiments, the interrogation source was produced by means of accelerators (or reactor) and the sample was moved from the irradiation chamber to the measurement station with a pneumatic rabbit.

The 14 MeV neutron or the delayed gamma lines emitted above 3 MeV are very penetrating and could be used to provide information about the inner part of the large UF_6 cylinders.

However, the transposition of such experiments to the UF_6 containers would require a feasibility study which would widely exceed a 2 to 4 year time frame prior to a possible implementation [1].

E. Specific investigations in respect to the design of an unattended measurement station for UF$_6$ containers

Introduction

The chapters C and D have shown that due to the experimental constraints such as gamma ray interference, Pa deposit, etc…, the ^{235}U enrichment can be determined only by means of a high resolution detector or with passive/active neutron measurement techniques, whereas the UF$_6$ mass can be checked using passive neutron measurements.

In this context, the purpose of this chapter is to provide answers to more specific queries such as:

1) Concerning the ^{235}U enrichment:

- The most important sources of uncertainty are due to the non-uniform wall thickness and to the low count rate. The contribution of the non-uniformity of the wall thickness was discussed in paragraph. C1.2.2.3. whereas the contribution of the count rate still needs to be evaluated. All the experiments cited in chapter C and D, the measurement were made with the detector as close as possible to the containers, what becomes the count rate at 50 cm for an optimized geometry?

- What about the use of the LaBr$_3$ detector?

- For passive neutron measurement, what is the most appropriate design for the detector and its measurement geometry? And what is the detector response as a function of the enrichment and as a function of the different UF$_6$ filling profile (section B2)?

2) Concerning the UF$_6$ mass determination:

- Can MCNP calculations confirm that the neutron leakage factor is almost constant for large changes in enrichment and cylinder loading? Or in other words, do all the parts of the load contribute to the neutron signal?

3)-Concerning the active neutron measurement:

- What is the signal intensity and origin when irradiating a 48Y cylinder with a strong 14MeV neutron source?

The chapter E is subdivided in two sections to answer to these questions. The first is dedicated to the ^{235}U enrichment determination by gamma spectrometry whereas the second part is focused on MCNP calculations applied to passive and active neutron measurements.

E 1. Enrichment determination by gamma spectrometry

E 1.1. Use of a Germanium detector

Figure 10 shows measured spectra for depleted uranium in 48Y containers and 3.5 % enriched uranium in 30B containers [37]. The measurements were carried out using a GL1020R CANBERRA detector (diameter 3.6 cm, length 2 cm) with a front collimator with a 4 cm opening diameter and a 1.5 cm length. The 185.7 keV line count rate was around 43 cps for the 30B containers and 2 cps for the 48Y. With these measurements the collimator was in contact with the cylinder.
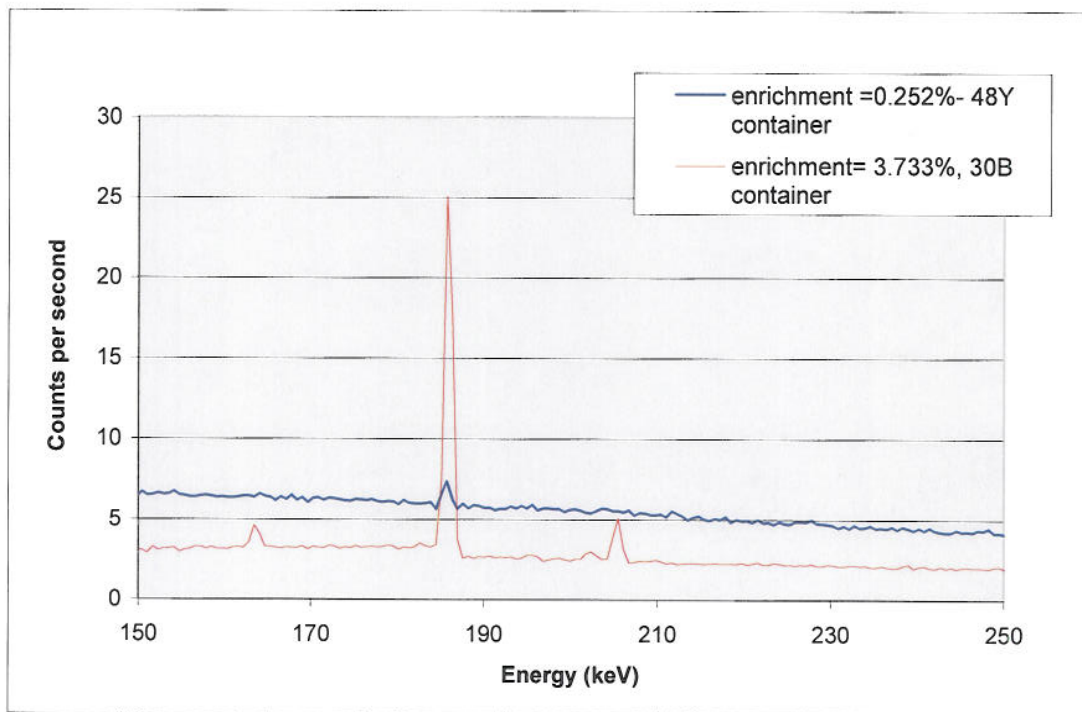
Figure 10: Depleted and LEU measured with a germanium detector

For the measurements with m = 50 cm space between collimator and drum, the net peak count rate was estimated with a simple model. It consists of the following elements (figure 11):

- a detector which is described by its crystal diameter d,
- a thick ("black") lead collimator with a diameter c,
- a distance l between collimator and detector crystal,
- a distance m = 50 cm between collimator and drum,
- the detector "sees" only an area with a diameter f = 40 cm on the drum surface (30B, f = 70 cm for 48Y),
- behind this area, the infinite thickness condition is always fulfilled (measure from below, e.g.),
- the attenuation in the container wall.

For this model the parameters l and c were optimised to get the maximum possible count rate such that it is then proportional to $d^2 * (c/l)^2$, i.e. proportional to the detector area and to the solid angle of the observed source region (which appears inside the collimator opening).

For the large germanium detector GL3825R of CANBERRA with 6.9 cm diameter (and m = 50 cm), the maximum count rate is achieved with a collimator of c = 11 cm diameter in l =31cm distance from the detector crystal for the 30B container. For the type 48Y it is possible to use the emission from a larger area with f = 70 cm, in which case the optimum parameters are c =16 cm and l = 26 cm.
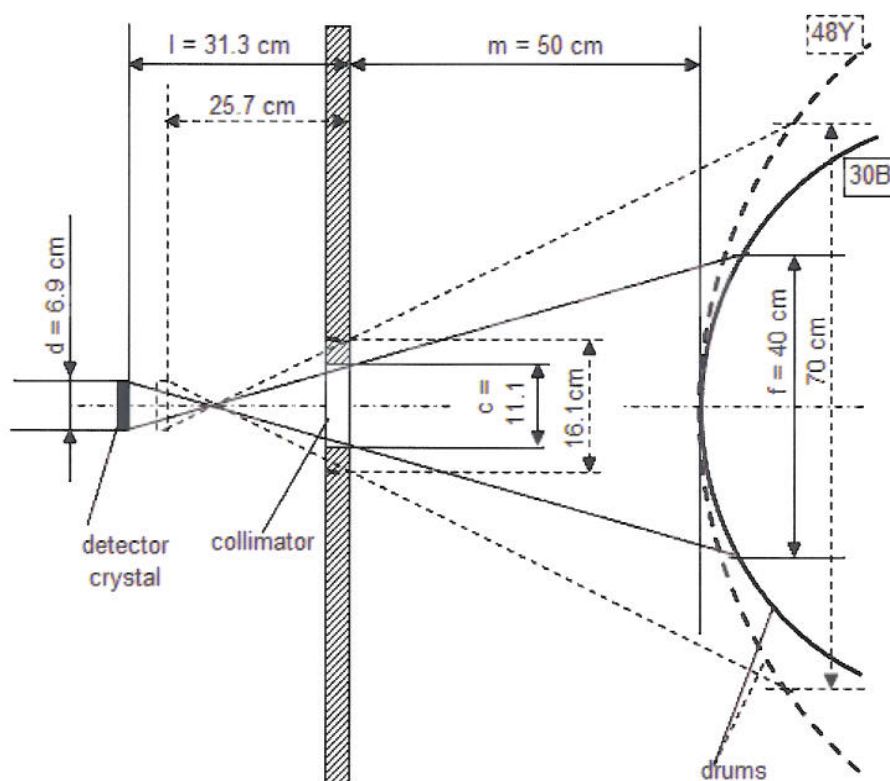
Figure 11: Parameters of the measurement geometry

Table 12 shows the estimated count rates and the associated random error u(r) for this very large detector and the optimised collimator.

	30B container	48Y container
Enrichment (%)	3.5	0.252
f	40	**80**
d	6.95	6.95
l	31.3	19.72
c	11.2	17.64
Count rate (cps)	**<10**	**<3**
u(r) % for tc=300s	20	30

Table 12 Estimated count rates and associated random error at 50 cm distance

Results show that the relative random uncertainty component u(r) is much above limits mentioned in the specifications R13 of [1] (u(r) = 4% for LEU products and u(r) = 5 % for NU and u(r)= 15 % for DU tails) for the maximum counting time (t_c = 300 s).

E 1.2. Use of a LaBr$_3$ detector

The newly developed LaBr$_3$ scintillation detector [48] is characterized by a resolution of 3.5% at 662 keV.

A 1.5 * 1.5 inches LaBr$_3$ detector with an efficiency comparable to that of a coaxial germanium detector (diameter 5.2cm depth 5.2 cm) [4] was recently tested in the PERLA laboratory [49] and in the field on 48Y and 30B containers [38]. The measurements were made in contact with the containers.

Figure 12 show spectra of depleted and low enriched uranium taken with the LaBr$_3$ detector equipped with a front collimator of 4 cm diameter and a 1 cm length.

One can see that due to the resolution, the spectra analysis requires the application of fit techniques.
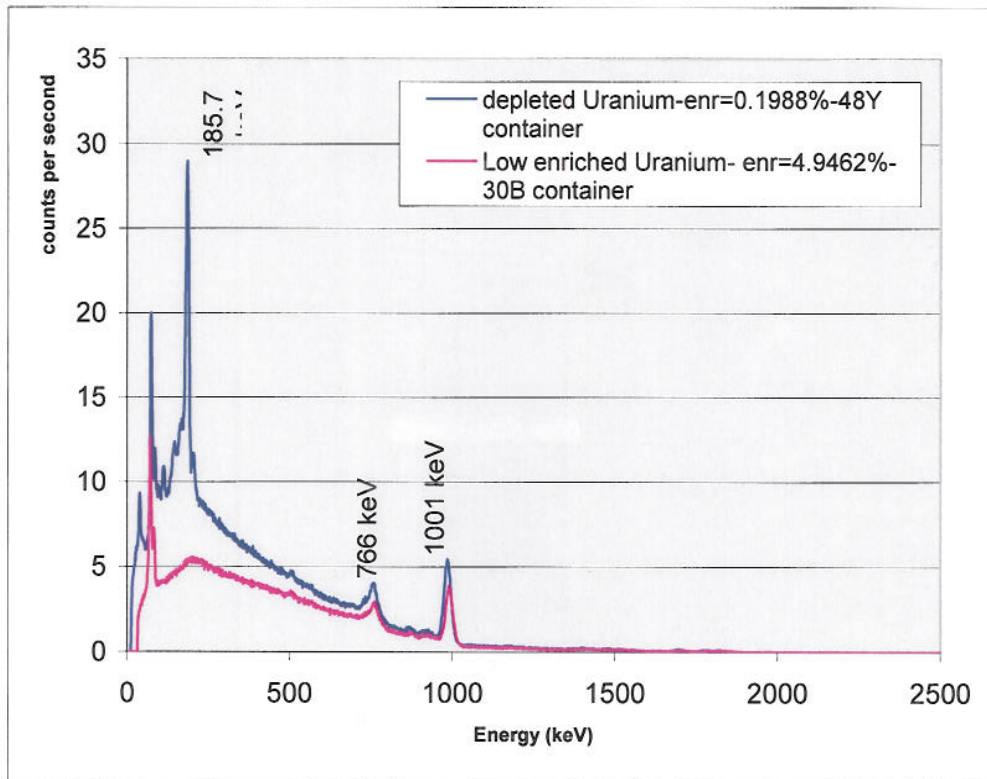
Figure 12: Depleted and LEU measured with a LaBr₃ detector

The analysis carried out in [49] showed that:

- the signal peak/background is too weak for the enrichment determination for depleted uranium in 48Y containers in the given experimental conditions,

- the 185 .7 keV line count rate is equal to 256 counts/second for a 5% enriched cylinders when the detector is in contact with the cylinder wall.

It is possible to optimise the geometry to get the highest count rate at 50 cm distance from the containers. If we assume furthermore that the size of commercially available LaBr₃ detectors grows, it might become possible to fulfilling the requirement R13 of [1]. However, the problem of the wall thickness correction persists and the small systematic errors mentioned in the requirement R13 of [1] cannot be achieved.

E 2. Calculation of the neutron detector response for passive measurements

In [7], the response of ^{3}He detectors due to emission of neutrons from UF$_6$ containers was calculated for four neutron detectors arranged around the steel container (fig.14). The detectors are in fixed positions for both containers at 60 cm distance and at mid height of the axis of the containers.
Each detector comprises 5 ^{3}He tubes of 2.54 diameter and 1meter active length (fig.14) with a pressure of 4 atm.

The neutron count rate of this set-up can be evaluated in different directions: either to determine the enrichment (in this case, the UF_6 mass and the $^{234}U/^{235}U$ ratio need to be known) or to determine the UF_6 mass (here, the enrichment and the $^{234}U/^{235}U$ ratio need to be known).
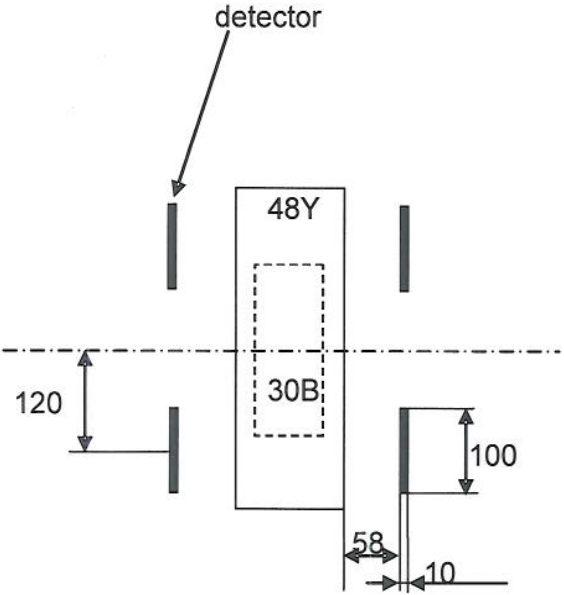
Figure 13: Measurement geometry for passive neutron measurement (dimension in cm)
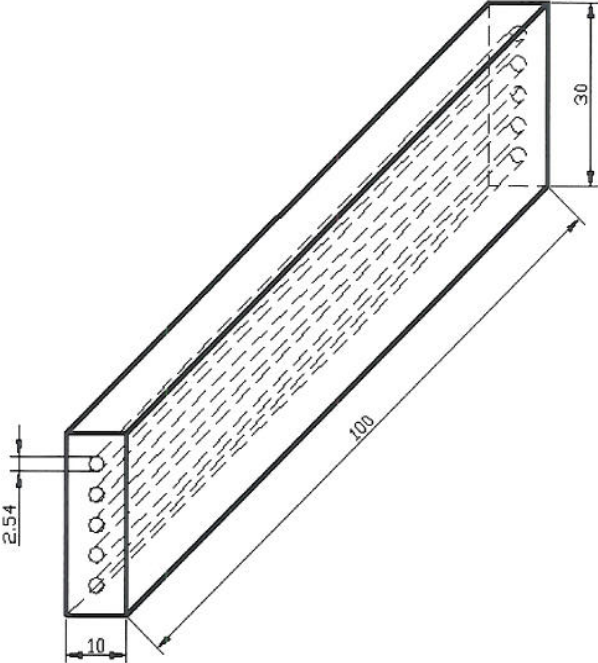
Figure 14: Schematic drawing of the detector (dimension in cm)

The relation between the detector response and the fuel enrichment or the total UF$_6$ mass was investigated for the containers types 30B and 48Y. Since the UF$_6$ filling profile is not known a priori five different fuel filling profiles– numbered from 1 (x=0) to 5 (x= 100) were taken into account (fig15). They cover the two cases described in figure 6a and 6b of section B2. The parameter x represents the percentage of UF$_6$ covering all the inner cylinder walls with a layer of constant thickness. The rest of the material fills the remaining volume from below.

The simulations were made for eight different isotopic compositions including that of reprocessed material (table 13).

The neutron flux in the vicinity of the containers was also investigated up to a distance equal to 300 cm.

All together, 60 computational cases were considered. The ratio of the flux values at the detector position and at 300 cm distance from container surface is at most 20% (Annex 3)

No	Material type	^{232}U	^{234}U	^{235}U	^{236}U	^{238}U	^{234}U/^{235}U
1	Natural	0	0.0056	0.718	0	99.2764	0.007799
2	Dep03	0	0.00234	0.3	0	99.69766	0.0078
3	LEU10	0	0.0078	1	0	98.9922	0.0078
4	LEU30	0	0.0234	3	0	96.9766	0.0078
5	LEU50	0	0.039	5	0	94.961	0.0078
6	Repro 6.49%	1.20E-08	0.067	6.471	0.05	93.462	0.010354
7	Sample 3.25%	4.80E-07	0.085	3.25	1.09	96.665	0.026154
8	Sample 5 %	7.60E-07	0.133	5	1.55	94.867	0.0266

Table 13: Isotopic composition used in MCNP calculations (in wt %)

Figure 15: UF$_6$ filling profiles

E 2.1. Calculation of neutron source and neutron spectrum

The neutron sources are calculated for the eight fuel compositions of Table 11. The neutrons are released by (α,n) reactions and spontaneous fission. The neutrons from (α,n) reactions are calculated with the code ALPHAN which is part of the ORIGENJR code [50]. The (α,n) reaction rate per unit time and unit volume is given by:

$$\Delta N = n_T \sigma_T (E_\alpha)\Phi(E_\alpha)\Delta E_\alpha ,$$

where E_α is α-particle energy in L.M.S., n_T is number density of target nuclei (here ^{19}F), σ_T is total cross section of (α,n) reaction and Φ is the scalar flux of a-particles. The α-particle energy is calculated for 100 points from 10 to 1 MeV with an equal spacing of energy. Neutron energy groups are 200 from 14.9 to 0.1 MeV with a lethargy width of 0.025. The neutron energy spectrum from spontaneous fission follows a Maxwellian distribution. The neutron sources for the eight fuel compositions related to 10^6 g of UF_6 are presented in Table 3.

E 2.2. Calculation of neutron detector response

For the container 30B all fuel compositions were taken into account whereas for the 48Y container, only the compositions 1, 2, 3 and 7 of table 11 were considered. The neutron flux and the detector response were calculated with the Monte Carlo code [52] and all the neutron cross sections were taken from the ENDF/B VI.1 and ENDF/B VI.O library. Table 14a and 14b give the detector response calculated as the sum over the four neutron detectors for both container types. The statistical uncertainty was always less than 1%.

No.	Compostion	Detector response 1/s				
		x=0	x=25	x=50	x=75	x=100
1	Natural	1.872E+02	2.316E+02	2.589E+02	2.809E+02	2.941E+02
2	Dep03	1.301E+02	1.620E+02	1.796E+02	1.939E+02	2.075E+02
3	LEU10	2.235E+02	2.803E+02	3.109E+02	3.400E+02	3.576E+02
4	LEU30	5.152E+02	6.469E+02	7.049E+02	7.722E+02	8.115E+02
5	LEU50	8.282E+02	1.027E+03	1.136E+03	1.211E+03	1.292E+03
6	Repro 6.49%	1.410E+03	1.748E+03	1.924E+03	2.029E+03	2.145E+03
7	Sample 3.25%	1.807E+03	2.239E+03	2.474E+03	2.640E+03	2.817E+03
8	Sample 5%	2.850E+03	3.507E+03	3.822E+03	4.101E+03	4.410E+03

Table 14a: Detector response for the container 30B

No.	Compostion	Detector response 1/s				
		x=0	x=25	x=50	x=75	x=100
1	Natural	1.008E+03	1.268E+03	1.420E+03	1.548E+03	1.625E+03
2	Dep03	6.909E+02	8.691E+02	9.766E+02	1.070E+03	1.115E+03
3	LEU10	1.209E+03	1.550E+03	1.723E+03	1.888E+03	1.984E+03
7	Sample 3.25%	1.009E+04	1.255E+04	1.413E+04	1.524E+04	1.609E+04

Table 14b: Detector response for the container 48Y

One can see that the detector response depends very much on the filling profile as it increases from filling profile x=0 to x=100 by a factor of 1.6.

A minimum of 156000 counts and 828000 counts for two minutes are calculated for the 30B container and for the 48Y respectively as a sum over four ^{3}He detectors. The potential background contribution of a drum at 300 cm distance is 20 % of the total neutrons signal, but it can be reduced substantially by appropriate shielding of the detector. Monitoring of background radiation in the environment of the measurement station may be used to make automatically background corrections.

### E 2.2.1. Detector response as a function of enrichment

The detector response is, like the neutron source strength, a linear function of the ^{235}U wt%. The Figures 16a and 16b show the detector response as a function of ^{235}U wt%, for different filling profiles and for both containers. The gradient of the functions increases from x=0 to x=100. The equally thick layer of UF_6 on all internal surfaces gives the highest detector response. The dependence of the detector response on the geometry is illustrated in figure 17 for the 48Y container.

In principle, the relation between the count rate R, UF_6 mass and the enrichment f_{35} can be approximately described by the formula:

$$R = Z(M_{UF6}) * (c + d \cdot f_{35})$$

The function Z and the parameters c and d depend on the container type and the specific set-up of the measurement station.

Because of the strong dependence of the detector response on the filling profile, the filling profile has to be known in order to determine the ^{235}U wt% from the detector response. Otherwise, e.g., depleted Uranium cannot be distinguished from 1% enriched U (48Y) or 3% from 5% (30B), in unfortunate cases.
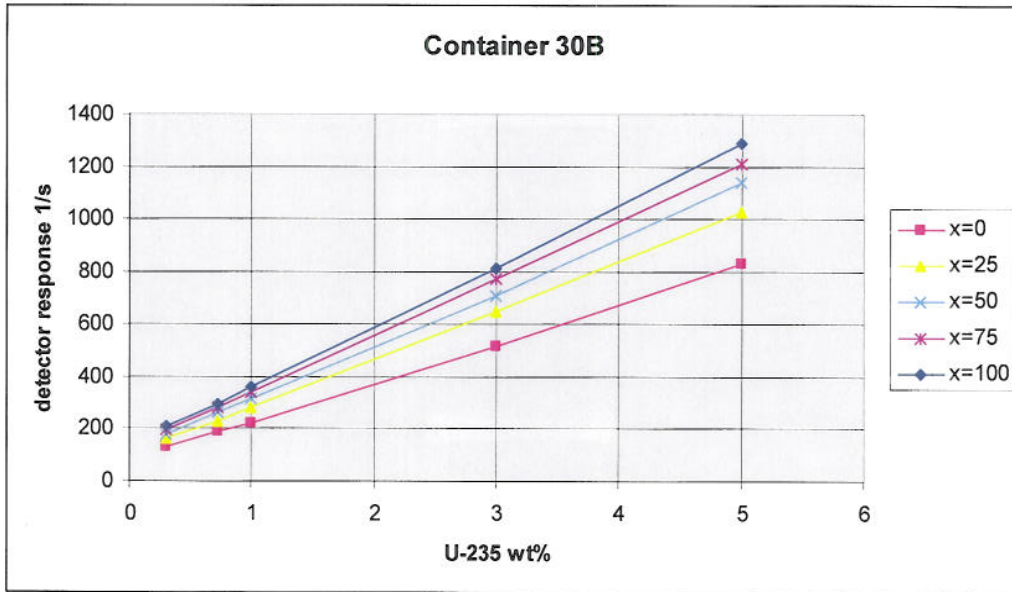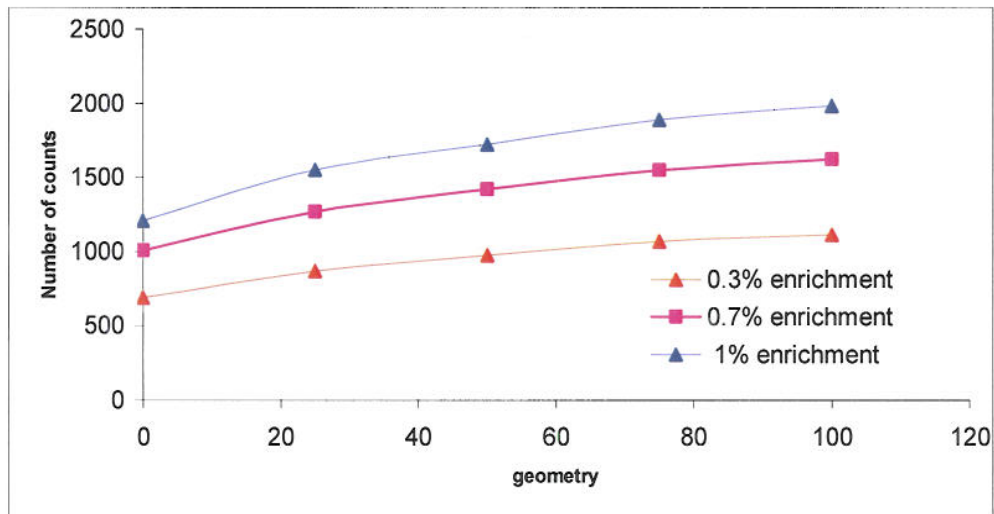
Figure 16a: Dependence of the detector response on the ^{235}U wt% for container 30B
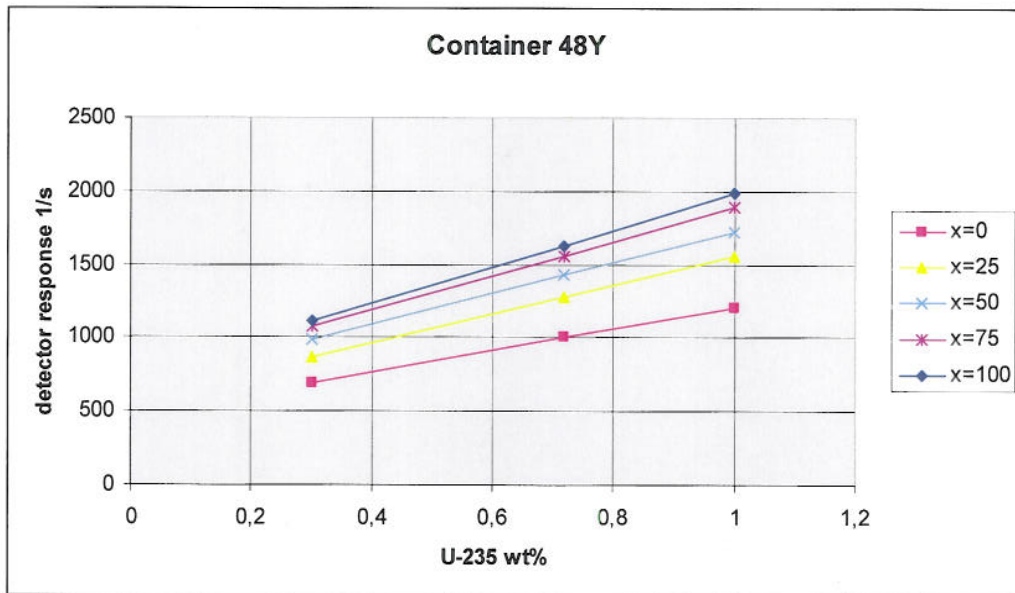
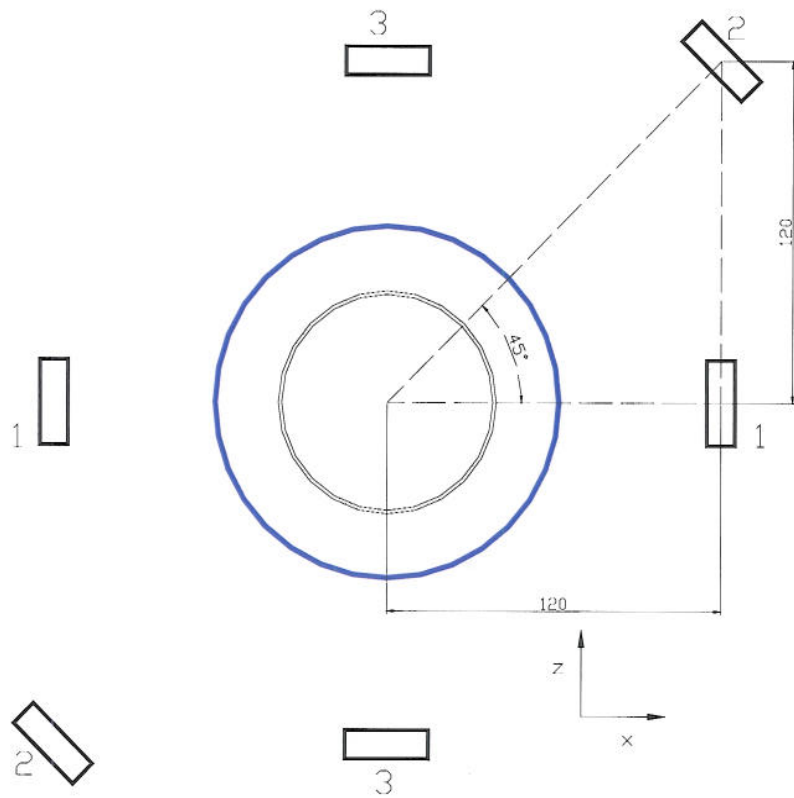**Figure 16b:** Dependence of the detector response on the ^{235}Uwt% for container 48Y

Figure 17: dependence of the detector response on the filling profile

E 2.2.2 Influence of detector positions [51]

In order to reduce the strong dependence of the detector response on the filling profile, the detector positions were changed. In comparison to [7] (detector position 1) two different detector positions are considered. At first the lateral distance of the detectors from the containers is fixed but the detectors are shifted in z-direction by 120 cm and -120 cm respectively and rotated by 45° (position 2). In the second case the detectors are positioned 120 cm above and below of the containers and rotated by 90° (position 3). The Figure 18 shows an x-z cross section through the container with the positions of the detectors.

Figure 18: x-z cross section trough the containers with position of detectors (in cm)

The calculated detector responses for the three detector positions are given in Figure 19a and 19b. The detector positions 2 and 3 clearly reduce the dependence of the detector response on the filling profile where the position 3 shows the highest detector response. Because of he rotation symmetry the detector positions 1 and 3 give the same values for the filling profile x=100.
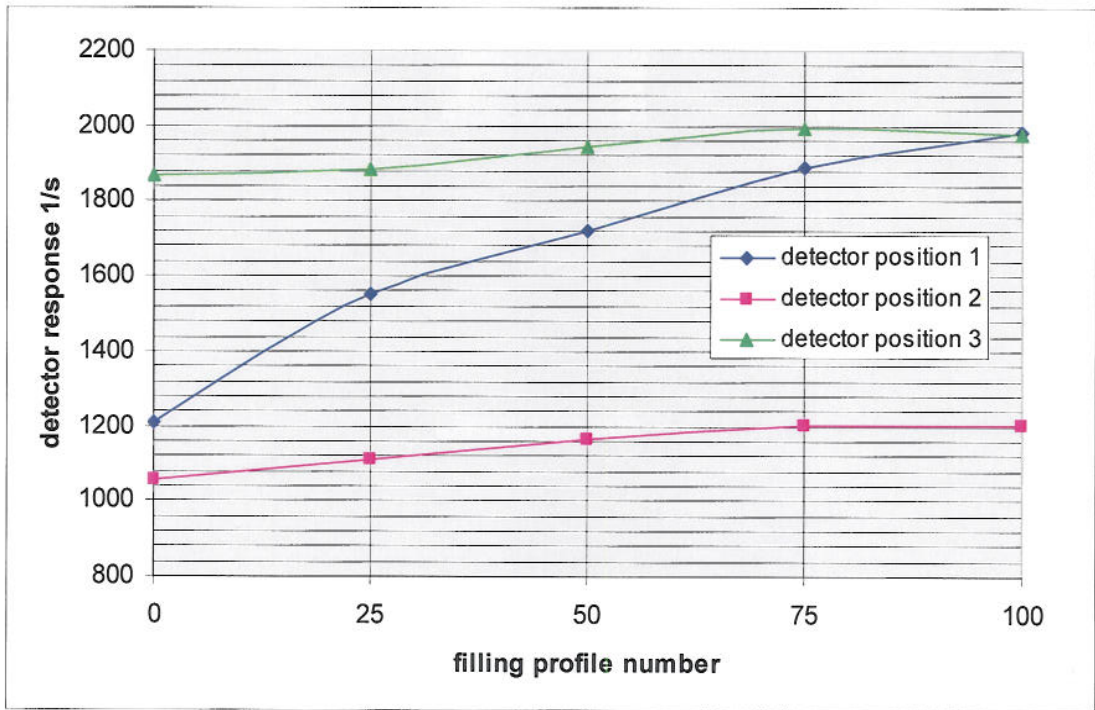
Figure 19a: Detector response for container 48Y
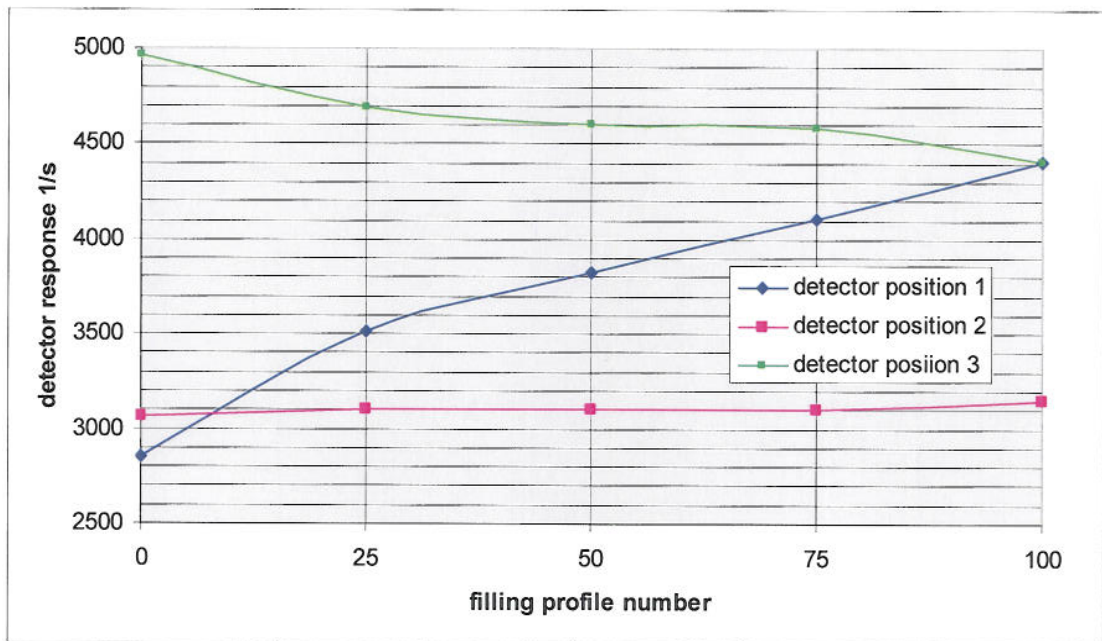
Figure 19b: Detector response for container 30B

The strong dependence of the detector response on the filling profile can possibly be reduced by shifting the detectors in the x-z-plane (see figure 18). A shift only in z-direction reduces the influence of filling profile but also decreases the detector response. A shift in z- and x-direction (x=0) reduces the influence of filling profile and increases the detector response. Further optimization calculations can be made but they are of interest only if they take into consideration the local conditions of a possible measurement station, taking into account both scattered radiation and the possible presence of other UF_6 containers in vicinity of the measurement station.

E 2.2.3. Contributions of the volume elements inside the container

If the detector response is written as:

$$R = Z(M_{UF6}) * (c + d \cdot f_{35})$$

the function $Z(M_{UF6})$ has to be evaluated for a given container.

For the calculation of the contributions of different UF_6 volume layers to the detector response of a 100% filled container, the UF_6 volume was divided into four volume layers. Only the filling profiles x=100 and x=50 were considered, where the description of the filling profiles is taken from [1]. The volume layers are numbered from 1 to 4 as shown in the Figure 20a and 20b.
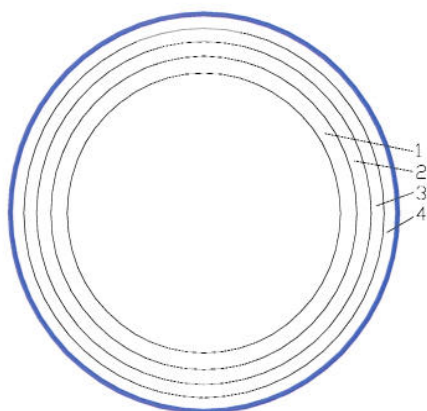
Figure 20a:	**Figure 20b:**
x-z cross section of the UF_6 volume layers	x-z cross section of the UF6 volume layers
for the filling profile x=100	for the filling profile x=50

All volume layers have the same UF_6 mass, 3.0E+06 g for container 48Y and 5.5E+05 g for container 30B. For the calculation of the detector response the detector positions are the same as in [7]. The results calculated with the MCNP code are represented in Table 15.

| filling profile No. | layer No. | detector response contribution % | |
		48Y/LEU10	30B/Sample 5%
100	1	20,3	23,4
	2	22,8	24,5
	3	26,6	25,2
	4	30,3	26,9
50	1	31,8	29,3
	2	34,6	30,5
	3	8,6	15,4
	4	25,0	24,8

Table 15: Contributions of volume layers to the detector response for geometry 1

For the filling profile x=100 all four layers are contributing in a similar way to the detector signal. None of them is "invisible". For the filling profile x=50, the figures point clearly on the least visible volume element, namely number 3.

E 2.2.4. Detector response to partially filled drums

The assumed filling processes were mentioned in chapter B2. The filling by de-sublimation corresponds to the filling profile x=100 whereas the filling at 80 degrees Celsius corresponds to the filling profile x=50. Figures 21a and 21b show the relative detector response as a function (constant * Z(Muf6)) of the filling state.

$$y = -8E-06x^2 + 0.0622x + 0.2486$$

$$y = -4E-06x^2 + 0.0536x - 0.275$$
$$R^2 = 0.998$$
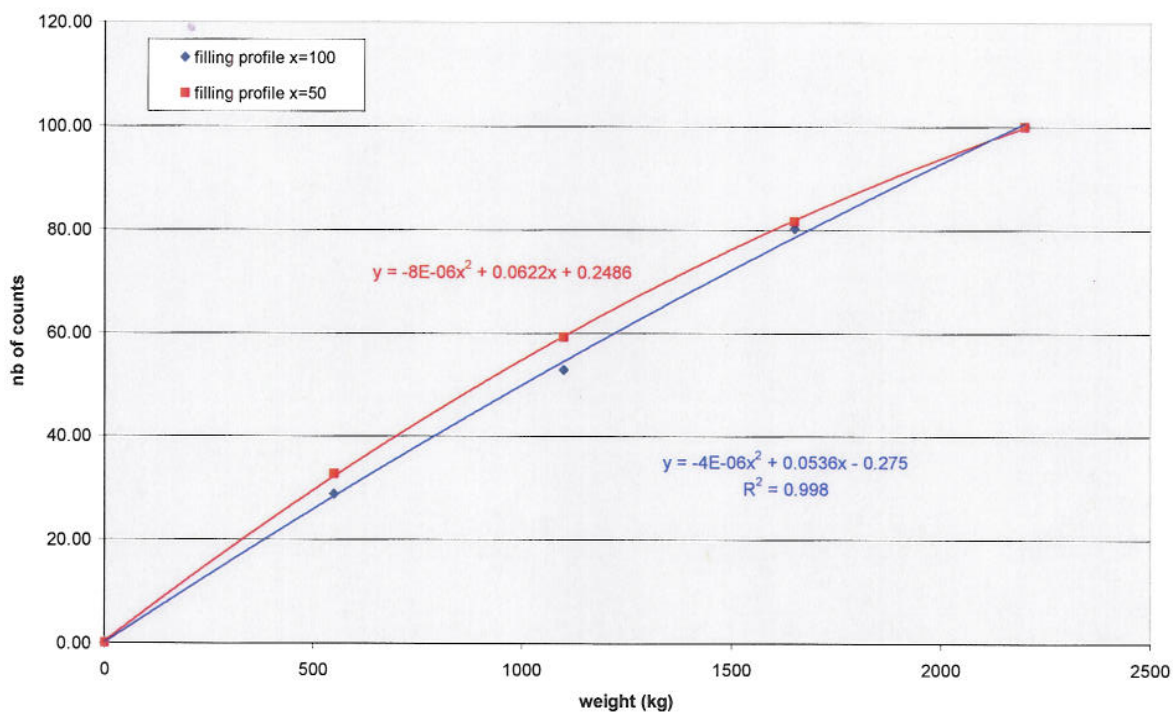
Figure 21a: nb of counts= constant *Z(MUF_6) for a 30B container, 5% enrichment
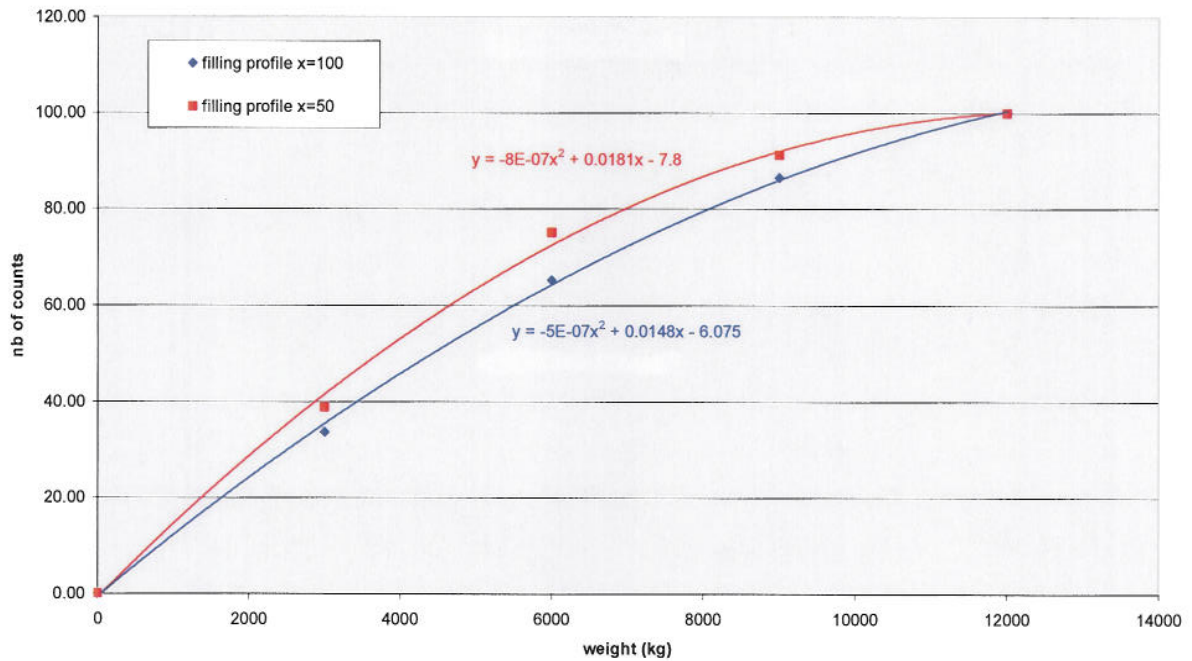
Figure 21b: number of counts= constant *Z(MUF_6) for a 48B container, 1% enrichment

The function $Z(M_{UF6})$ can be fitted with a polynomial. It does not show a saturation effect. Consequently, the filling process could be supervised from beginning to the end in a filling station, in parallel to the observation of the container mass with a balance. One can see that a variation of 10% of the total mass would be translated by a change of more than 10% (x=100) and 8% (x=50) for the 30B containers. For the 48Y containers, a variation of 10% of the mass would results in a change of 7% (x=100) and 5% (x=50). It can be expected that the function $Z(M_{UF6})$ gets closer to a simple straight line for the detector positions 2 and 3.

To characterise once again the "visibility" of the UF_6 and its dependence on the filling profile, the neutron leakage fraction was calculated from table 14. Results were arbitrarily normalised to 1 for an UF_6 weight equal to one fourth of the total load for both container types. Fig 22a and 22b show that the leakage fraction remains quite high also for the large drums and demonstrate the clear effect of the filling profile.

We observe small variations of the leakage fraction as a function of the UF_6 mass and confirm by this way experimental results of ref 6: in this paper, the authors measured a leakage factor varying from 0.93 to 0.82 as the weight of the 2 ½ enriched UF_6 is increased from 2000 to 5000 lb for a filling profile which is not described. The ratio of the leakage fraction for 5000 lb over the leakage fraction for 2000 lb gives 1.13.
Taken the results of the present document, the corresponding ratio becomes equal to 1.09 and 1.23 for x= 100 and x=50. Since we can easily imagine that the filling profile of [6] is something in-between x=100 and x=50, there is a very good agreement between the results of the present simulation [7] [51] and the experimental results of [6].
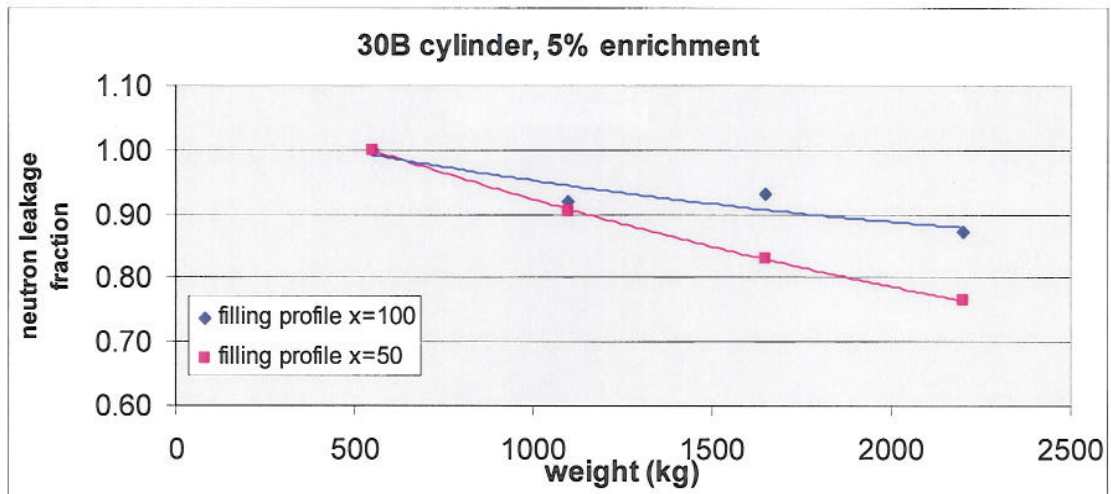
Figure 22a: neutron leakage fraction for a 30B container filled with 5% enriched UF_6
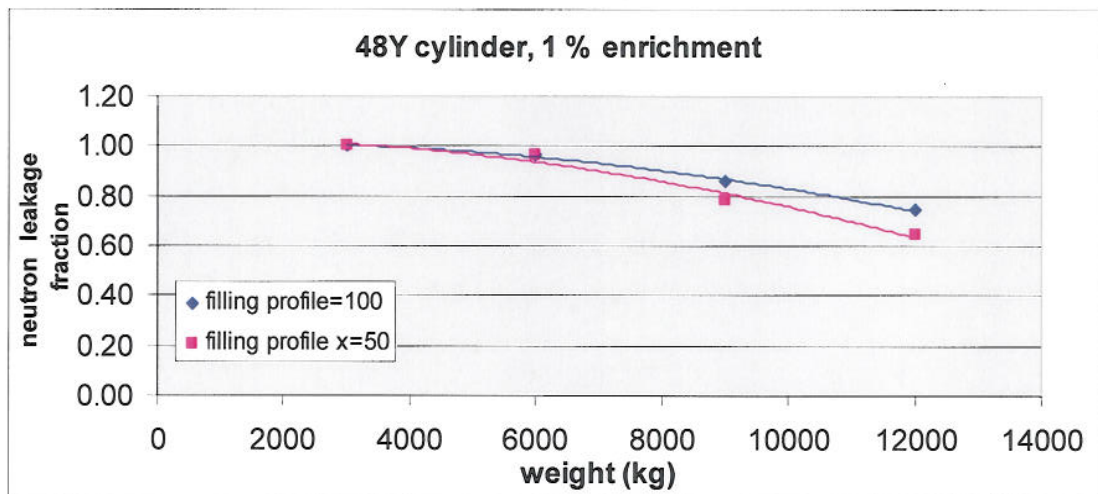
Figure 22b: neutron leakage fraction for a 48Y container filled with 1% enriched UF_6

E 2.2.5 Active methods

The purpose of this section is to evaluate the individual contribution of each isotope to the neutron signal induced by irradiation with a 14 MeV neutron source, and to estimate the required source strength of an external neutron source.

For active measurements a 14 MeV neutron source is positioned below the centre of the container in a distance of 60 cm from the container surface. A direct path between the neutron source and neutron detectors is shielded. So neutrons can only indirectly reach the detectors. In a first step the fission sources for ^{235}U (thermal and epithermal) and ^{238}U (epithermal) are calculated. Because the fission source in the container is space dependent, the UF_6 volume has to be divided in space zones. The investigations have shown that a large

number of space zones is necessary. For the filling profile x=50 the UF_6 volume is divided in 275 discrete volumes (11 axial zones and 25 zones in the container cross section vertical to longitudinal axis). The boundary between the thermal and the epithermal energy region is 10 eV.

With the space depended fission source the detector response is calculated in a second step. The results for the computational cases 48Y/LEU10 and 30B/LEU50 and 14 MeV neutron source strength of 10^8 n/s are presented in Table 16.

computaional case			detector response 1/s					
cont. type	compo-sition	filling profile	U-235 thermal	U-235 epithermal	U-238 epithermal	fission total	all without fission	total
30B	LEU50	x=50	1,969E+01	4,608E+03	1,139E+04	1,602E+04	1,955E+04	3,558E+04
48Y	LEU10	x=50	3,916E+01	1,747E+03	7,042E+03	8,828E+03	1,356E+04	2,239E+04

Table 16: Detector response for 14 MeV neutron source strength of 1.0E+08 n/s

In the last but one column of Table 3-1 all reactions without fission (scattering, (n, 2n)) are summed up. These neutrons give the highest contribution to the detector response. The fission contribution is mainly determined by the ^{238}U epithermal fission neutrons. Only 29% and 20% for 30B/LEU50 and 48Y/LEU10 respectively come from ^{235}U fission.

An external neutron source of 14 MeV below the containers results in an internal neutron source in the UF_6 fuel caused by fission and non fission (scattering and (n, 2n)) reactions. This neutron source is strongly space depended. With the space depended neutron source the detector response was calculated. With a neutron source strength (14 MeV) of 10^8 n/s the detector response is higher in comparison of passive measurements by more as a factor of 30 and 10 for 30B/LEU50 and 48Y/LEU10 respectively. The detector response is not very sensitive to the ^{235}U content of the UF_6 fuel because the main fission source contribution comes from ^{238}U fission. In addition the fission source only provides 40 – 45 percent of the total neutron source.

E 3. Informatics means for unattended operation

The practical implementation of unattended measurements can be done with existing informatics solutions. The system RADAR of EURATOM can integrate all measurements of photons and neutrons discussed here and combine it with other information such as automatically read container numbers, drum weights from a balance background radiation from a monitoring detector etc. It is a flexible system which can be adapted to site specific tasks and local conditions for data collection.

The data evaluation systems for the RADAR data, CRISP or XSEAT, are also sufficiently flexible to be adapted to extra needs such as the integration of time dependent background radiation correction on the basis of background monitoring detectors. The data are accessible online. These informatics solutions have been routinely used by EURATOM for many years and work reliably.

Conclusion

It has been shown in Chapter E1 that the ^{235}U enrichment measurement by gamma spectrometry does not allow fulfilling the requirement R13 of [1] as the 6% systematic error due to the non-uniform wall thickness is too much above the required 2% (C 1.2.2.3.). Even very large germanium detectors at 50 cm distance from the cylinder provide such a low net peak count rates that the random error also remains above the requested limit. Large LaBr$_3$ detectors may deliver higher count rates and reduce like this the random uncertainty u(r) below the requested 4% for LEU. However, for depleted uranium and for tails, the 185.7 keV line is below the detection limit because of its tails.

In contrast, the calculations carried out using the Monte Carlo radiation transport simulation code MCNP have shown that passive neutron measurements can be used to determine either ^{235}U enrichment or UF$_6$ mass provided that the ratio ^{234}f/^{235}f is known. The results depend strongly on the UF$_6$ filling profile, however, an effect which can be minimized by optimization of the detector position relative to the containers. The total number of counts is found to be a linear function of the ^{235}U enrichment (for 100% filled drums) and is also rather a linear function of the UF$_6$ mass (for partially filled drums). In a scenario whereby 10% of the UF$_6$ mass would be missing from the cylinder, the total number of neutrons would also diminish by nearly 10% for both container types. At least 156000 counts and 828000 counts are collected, for the 30B container and for the 48Y respectively, as a sum over four ^{3}He detectors (without back shielding) in two minutes acquisition time. The potential background contribution of a drum at 300 cm distance is 20 % of the total neutrons signal. Finally, the activation with a 14 MeV generator has shown that the resulting signal is not very sensitive to the ^{235}U content.

F Summary

The indications written in bold between brackets refer to the requirements listed in [1].

This work has surveyed the state-of-the-art NDA methods applicable to the determination of the ^{235}U enrichment and the UF$_6$ mass in 30B and 48Ycontainers and defined the measurement possibilities within the constraints listed in [1], i.e.:

- The NDA method, or combination of methods will accurately determine the enrichment (**R1 and R13**) of ^{235}U , confirm the quantity in UF$_6$ (**R2 and R14**) and assay the homogeneity of the UF$_6$ (**R3**),
- The NDA methods and supporting hardware must allow unattended operation (**R4 and R15**),
- The cylinder to detector distance must be at least 50 cm to allow safe movements of the cylinders (**R5**),
- The minimum distance between the assayed cylinder and another cylinder is 3 metres (**R6**)
- Cylinders must be assayed at different temperature(**R7**),
- The NDA methods must be applicable to "fresh" uranium as well as uranium recovered from spent fuel (**R9**),
- The measurement must be completed within 5 min (**R16**).

It has also been shown here that:

1) The ^{235}U enrichment determination by gamma spectrometry cannot fulfil the requirements of [1] for the following reasons:

- the measurement is affected by the variation in wall thickness of the container which leads to a systematic error u (s) equal to 6 %.
- the count rate is too low at 50 cm distance for a germanium detector for both container types
- the count rate is high enough at 50 cm distance for LaBr$_3$ detector but this is true only for 30B container type

2) The enrichment and the UF$_6$ mass can be confirmed with passive neutron measurements for both cylinders types (R8) and uranium type (R9) provided that the $^{234}U/^{235}U$ ratio is known. This technique is not sensitive to the deposition of protactinium on the container inner wall. However, a false declaration of the ^{235}U enrichment, which can not be detected by gamma spectrometry, will escape detection by the inspectors, as the expected neutron count rate (corresponding to the false declaration), can be adjusted by simply compensating for the missing neutrons with HEU material hidden in the cylinder.

MCNP calculations have shown that:

- the results are sensitive to the filling profile. The influence can be reduced by optimization of the counting geometry (paragraph E.2.2.2.),
- the neutron count rate is a linear function of the enrichment for a given filling profile,
- the variations of the neutron leakage fraction as a function of mass or enrichment deviations are very small (paragraph E.2.2.3),
- 156000 counts and 828000 counts can be collected in two minutes for the 30B container and for the 48Y respectively as a sum over four ^{3}He detectors for the geometry defined in E 2.
- for an unshielded neutron detector, the potential background contribution of a neighbouring cylinder at 300 cm distance is up to 20% of the total neutrons signal.
- If 10% of the UF$_6$ mass would be missing in the cylinder, the neutron count rate would be diminished by a similar percentage for both container types.

3) Active neutron measurements with thermal neutrons allow to determine the ^{235}U enrichment without knowing the $^{234}U/^{235}U$ ratio. However, this seems to be possible only with source and detector in contact to the cylinder wall. MCNP calculations for the 14-MeV generated neutrons have shown that the detector response is not very sensitive to the ^{235}U content of the UF$_6$ fuel because the main fission source contribution comes from ^{238}U fission. In addition the fission source only provides 40 to 45 percent of the total neutron source. Active methods can not be used in short time.

4) It is not possible to check the radioactive homogeneity of the containers neither with gamma spectrometry nor with neutron techniques.

References

[1] A. Lebrun
User Requirements "state of the art NDA methods applicable to UF6 cylinders",
SG-EQ-NDA-UR 0001, 2007

[2] S. Richter, A. Alonso, W. De Bolle, R. Wellum, P.D.P. Taylor
Isotopic 'fingerprints for natural uranium ore samples
International Journal of mass spectrometry 193 (1999) 9-14

[3] Management of reprocessed Uranium   IAEA-TECDOC-1529, February 2007

[4] P. Mortreau, R. Berndt
Handbook of Gamma Spectrometry Methods for Non-Destructive Assay of Nuclear Materials, EUR 19822
EN , version 3, 2006
 http://nuclearsafeguards.jrc.it/nda/handbook3-2006.pdf

[5] P.E. Fehlau, W.H. Chambers   Perimeters Safeguards Techniques for Uranium enrichment plants,
LA-8997-MS, 1981

[6] R. B. Walton, T. Reilly, J. L. Parker and J. H. Menzel, E. D. Marshall and L. W. Fields
    Measurements of UF_6 cylinders with portable instruments,   Nuclear Technology, Vol. 21, February 1974

[7] E. Franke
Calculation of the neutron response for passive measurements-
Report-No UF6-01/08

[8] UF_6, a manual of good handling practices,
 USEC-651, revision 7, January 1995

[9] R. S. T. Shaw
The routine non-destructive measurement of the 235 U concentration   of enriched uranium
hexafluoride in transit cylinders using high resolution gamma spectrometry
Proceeding ESARDA 1979, Brussels

[10] P.G. Brown
Discussion of cause of UF_6 pressure excursions,
Proceedings, second international conference, Uranium hexafluoride handling, Oak
Ridge, 29-31. 1991

[11] Harry, R.J.S., Aaldijk, J.K.,Braak, J.K., 1976,

Spectrometric determination of Isotopic composition without use of standards, IAEA-SM-201/66 , Safeguarding Nuclear materials, Vienna, vol 11, p. 235

[12] R. Gunnink, R. Arlt, R. Berndt,

Proceedings of 19th Annual ESARDA symposium., Montpellier, France, May 1997

[13] J. Morel, M. Etcheverry and G. Riazuelo

Uranium enrichment measurement by X- and G-ray spectrometry with the "URADOS"

Process. Applied. Radiat. Isot. Vol 49, No9-11, p. 1251-1257, 1998

[14] T.E. Sampson, G.W. Nelson, and T.A. Kelley,

FRAM: A versatile code for analysing the isotopic composition of plutonium from gamma- ray pulse height spectra, Los Alamos National Laboratory.

Report LA-11720-MS (1989)

[15] T. Dragnev, V. Rukhov, D.E. Rundquinst, E. Szabo,

Combined Gamma and Passive X-ray Fluorescent Measurements of 235U and U-total concentration

Journal of Radio analytical and nuclear chemistry

Vol. 152, No.1, pp. 161-173, STR-264, IEAE, 1991

[16] Trinh K. L

Mesures d'enrichissement en ^{235}U d'echantillons uraniferes par spectrometrie gamma,

rapport de stage, 1994, IPSN/DSMR/SATE/GMMS, CEA-Fontenay –aux-roses

[17] S. Aboushal

Study of the MGAU applicability to accurate isotopic characterization of uranium samples,

NIM A 368(1996) 443

[18] A.N. Berlizov, V.V. Tryshyn

Evaluating factors limiting the accuracy of the isotopic characterization of uranium by the

MGAU method,   Workshop 2005, MGA FRAM IGA GXW, Karslruhe, Nov 14-16, 2005

IAEA-SM-367/14/05/P, 2001

[19] A.N. Berlizov, R. Gunnink, J. Zsigrai, C.T. Nguyen, V.V. Tryshyn

Performance testing of the upgraded uranium isotopics multi-group analysis code MGAU

NIM A575 (2007) 498-506]

[20] Ragimov, T.K., Rudenko, V. S. Petrov A.M., Timoshin V.I.

Study of the capabilities of the gamma-ray spectrometry method of determining the isotopic composition of uranium with the portable UPu Inspector gamma-ray spectrometer, MPC&A-2000, Obninsk, Russia

[21] D. T. Vo
FRAM's bias Workshop 2005, MGA FRAM IGA GXW,
Karslruhe, Nov 14-16, 2005

[22] D. Parise, M. Moeslinger, R. Carchon, M. Zendel,
Development of the GXW analysis software, Workshop 2005, MGA FRAM IGA GXW,
Karslruhe, Nov 14-16, 2005

[23] M. Moeslinger, D. Parise, R. Carchon
Evaluation of various Analysis Codes for the determination of Uranium Isotopes Workshop
2005, MGA FRAM IGA GXW, Karslruhe, Nov 14-16, 2005

[24] W. Ruhter, T. F. Wang, C. F. Hayden
Uranium enrichment measurements without calibration using gamma rays above 100 keV,
UCRL-JC-142832, Oct 29-Nov, 2001,

[25] E. Sampson, P. A. Hypes, L T Vo T.
FRAM Isotopic analysis of Uranium in thick-walled containers using high energy   gamma rays and
planar HPGe detectors
Proceedings, Institute Nuclear management, 2002

[26] T. D. Reilly, R.B. Walton, J. L. Parker
Nuclear Safeguards Research and development
LA- 4605-MS, pp. 19-21, Los Alamos Scientific Laboratory, 1970

[27] A.R. Flynn,
Field determination of uranium -235 enrichment by portable gamma ray spectrometry,
Report K-1819-1972,

[28] R. C. Hagenauer, H.Y. Rollen and J. M. Whittaker, R.L. Mayer, T. Biro,
Non-destructive measurement of UF_6 cylinders at the Portsmouth gaseous diffusion plant,
Nuclear   material management- annual meeting, 1998

[29] R. Gunnink, R. Arlt
Methods for evaluating and analyzing Cdte and CdZnTe Spectra
NIM A 45892001) 196-205

[30] P. Mortreau, R. Berndt
Determination of 235U enrichment with a large volume CZT detector
NIM A 556 (2006) 219-227

[31] J. B. Montgomery

Enhanced techniques and improved results in ^{235}U enrichment measurement of large UF_6 Cylinders by portable germanium spectrometer

Journal of nuclear materials management, 2006, volume 24, No 2

[32] E. Dermendjiev, N. Beyer, D. E. Rundquist

Non-destructive measurements of UF_6 stored in 5" and 30" cylinders

Proceedings of Annual ESARDA symposium, 1979

[33] SG-CP-20 IMCG uranium Enrichment in UF6 Cylinders Rev3

[34] F. Gabriel, A. Wolf, D. Proehl, R. Jainsch, K. W. Leege

Mini MCA-Evaluation, Field test and Commercialization

Esarda proceedings, Montpellier, 1999

[35] P. Mortreau, R. Berndt

Determination of the uranium enrichment with the NaIGEM code

A 530 (2004) 559-567

[36] P. Mortreau, R. Berndt

Attenuation of a non-parallel beam of gamma radiation by thick shielding – application to the determination of the ^{235}U enrichment with NaI detectors,

NIMA 43823, 2005

[37] P. Mortreau, R. Berndt

Measurement campaign on UF_6 containers at Georges Besse 1, 1997

[38] P. Mortreau, R. Berndt

^{235}U enrichment determination of UF6 containers with a $LaBr_3$ detector, 2008

[39] J.T. Caldwell

New Technique for ^{235}U enrichment determination in UF6 cylinders

Nuclear material management, vol 2 pt.2, 1973

[40] W. L. Myers, C. A. Goulding, C. L .Hollas

Determination of the ^{235}U enrichment of bulk Uranium samples using delayed neutrons

Physor 2006, American nuclear society

[41] L. Lakosi, C. Tam Nguyen, J. Bagi

Photo neutron interrogation of low-enriched uranium induced by bremsstrahlung from a 4 MeV LINAC

NIM B (2007)

[42] G.R. Keepin, T.F. Wimett, R.K. Ziegler,
Phys. Rev. 107 (1957) 1044

[43] S.E. Binnaey, R.I. Scherpelz,
Nucl. Inst. and Meth. B 154 (1978) 413.

[44] E.B. Norman et al
Signatures of fissile materials: high-energy gamma rays following fission,
NIM A 521 (2004) 608-610

[45] F. Carrel, M. Gmar, F. Lainé, J. Loridoon, J. L.Ma, C. Passard,
Identification of actinides inside nuclear waste packages by measurement of fission delays gammas,
IEEE Nuclear science symposium, 2006

[46] D.H. Morse et al.
Photo fission in uranium by nuclear reaction gamma rays,
NIM B261 (2007) 378-38

[47] O. Halna Du Fretay, Private communication

[48] A. Iltis, M.R. Mayhugh, P. Menge, C.M. Rozsa. O. Selles, V. Solovyev
Lanthanum halide scintillators: Properties and Applications
NIM A 563 (206) 359-363

[49] P. Mortreau, R. Berndt
Uranium enrichment determination with LaBr$_3$ detectors
2008, to be published in NIM

[50] K. Koyama, N. Yamano, S. Miyasaka,
ORIGEN-JR: A Computer Code for Calculating Radiation Sources and Analyzing Nuclide
Transmutations,
JAERI-M 8229 (May 1979

[51] E. Franke
Calculation for the neutron detector response for passive and active measurements
Report-02/08

[52] J. F. Briesmeister,
MCNP-A General Monte Carlo N-Particle Transport Code (Version 4B)
LA-12625-M, 1997

Annex 1

User requirements-SG-EQ-NDA-UR-0001

User Requirements

State of the art of
NDA methods applicable to UF6 cylinders

Alain Lebrun Document Preparation	NDA Systems Engineer		2007-08-09
Dominik Pacala Cleared: QMS Compliance	UH:SGTS-TTS-Planning and Coordination	Pacala	2007-08-10
Vladimir Ryzhikov Content Approved	UH:SGTS-TAU-Resident NDA		2007-08-09
Mark Pickrell Implementation Approved	SH:SGTS-TAU	(Signature)	2007-08-16 (Date)

Summary:	This document specifies the requested performances and features of NDA systems to be studied in the framework of the task proposal 07/TAU-04 `` State of the Art of NDA Techniques Applicable to UF6 Cylinders". It also specifies the deliveries expected from that MSSP task.
Access:	AIIS (Authorized Instrumentation Information System)
Document owner:	TAU

1 Purpose and scope

Purpose: This document describes the specifications for the study to be carried our by Members State Support Programmes under the Sp1 task proposal 07/ TAU-04 " State of the Art of NDA Techniques Applicable to UF6 Cylinders" [1]

Scope: This document is to be used by MSSP contractors to formulate their offers and conduct the research program. The scope of this document is limited to indicating the expected performances and constraints applicable to the methods for selection purposes. Further detailed user requirement will be elaborated to support the design and production phases.

2 Introduction

The IAEA verifications at Enrichment Plants include Non Destructive Assay (NDA) measurements which are currently carried out attended.

The IAEA formulated the project of establishing a centralised unattended measurement station at Enrichment Plants able to identify and assay all UF6 cylinders in and out of the plant thus forming the basis for running a real time material balance system. Both ^{235}U and ^{238}U balances are needed.

Work has already been done on demonstrating the feasibility of unattended identification of the cylinders using laser technology.

Unattended weighing of the cylinders will provide extremely accurate measurement of the flow of UF6 material. To form the ^{235}U and ^{238}U balance, accurate enrichment determination by NDA is needed.

NDA is also meant to supplement weighing in giving additional assurance on the nature and quantity of weighed material within the cylinders. In other words "to make sure that what is measured is actually what is supposed being measured".

The timeframe for implementation is 2 to 4 years which implies that NDA techniques not necessitating long R&D programs will be given priority.

The document is divided into 2 parts. The first part "NDA method User requirements" indicates the features, performances and constraints applicable to the NDA method to be investigated in the course of the study. The second one details the specifications related to the study by it self in particular the deliverables.

3 Background

Several NDA methods based on the detection and analysis of radiations emitted by UF6 are known and applied for safeguards verification. It is in particular the case of enrichment determination based on X and gamma radiation emitted from ^{235}U, ^{238}U and ^{234}Pa (decay product of ^{238}U). There are two methods based on X and gamma radiations. The first one is a calibrated method interpreting the absolute strength of the 185 keV gamma ray from ^{235}U in a fixed and controlled geometry (infinite thickness conditions). The second one is an intrinsically calibrated methods interpreting ratios of X-rays from both ^{235}U and ^{238}U and thus not necessitating any calibration. Both methods give excellent results but have the drawback of analysing only a tiny area of the cylinder and to be very sensitive to the presence of a UF6 deposit on the cylinder internal walls. In views of unattended operation, the predictability of the location of such measurement is a significant weakness. Furthermore the control of geometry would be difficult to manage in the case of calibrated method and the thickness of the cylinder walls makes the intrinsically calibrated method difficult to use. Although effective enrichment determination based on X and gamma detection and analysis are probably not the ideal choice for unattended determination of UF6 enrichment in cylinders. In addition because UF6 reaches infinite thickness after only a few centimetres, gamma methods cannot support a credible verification of the total mass of uranium in the cylinders.

UF6 emits significant amounts of neutrons through various processes.

The predominant neutron source is generated by (α,n) reactions generated by α irradiation from ^{234}U on fluorine. As ^{234}U varies proportionally with ^{235}U concentration, neutrons from (α,n) reactions are directly proportional to the enrichment when detected in "infinite thickness conditions" (small detector located next to the cylinder). Total neutrons from (α,n) reactions vary also with the total UF6 mass when neutrons are detected away from the detector or with a large detector seeing the whole cylinder.

In the case of recycled uranium, the relationship between ^{234}U and ^{235}U depends on the initial enrichment and burnup of the fuel from which the recycled uranium originates.

Correlated neutrons are emitted by spontaneous fission process from ^{238}U and as the result of ^{235}U fissions induced by (α,n) neutrons. Correlated neutrons may also be produced as the result of ^{235}U fissions induced by an external source of neutrons like a neutron generator. In general, the mean free path of neutrons in UF6 is much longer than for X and gamma rays thus allowing assay of the bulk of the UF6 cylinders. However, because of this potential of travelling far away, neutron methods may be more impacted by background conditions than gamma methods.

As briefly indicated above, NDA methods based on neutron detection offer promising perspectives for the safeguards verification of UF6 cylinders.

68

	User Requirements	Version Date:	2007-07-25
IAEA International Atomic Energy Agency	State of the art of NDA methods applicable to UF6 cylinders	Version No.:	1
Department of Safeguards SGTAU	SG-EQ-NDA-UR-0001	Page:	5 of 7

4 NDA methods User Requirements

4.1 General Functionalities

R1. The NDA method or combination of methods will accurately determine the enrichment of uranium in UF_6 cylinders.

R2. The NDA methods will allow confirming the quantity of uranium in UF_6 cylinders.

R3. The NDA methods should assay the homogeneity of the UF_6.

4.2 Constraints

R4. The NDA methods and supporting hardware must allow unattended operation.

R5. The cylinder to detector distance will be at least 50 cm to allow safe movements of the cylinders.

R6. Although the measurement station will be isolated for the cylinder storage park, one cannot exclude circulation or temporary storage of a few cylinders in the vicinity.

    R6.a. The minimum distance between the assayed cylinder and another cylinder will be 3 meters.

R7. Cylinders may be assayed at various temperatures and presence of UF_6 under liquid phase cannot be excluded.

4.3 Performance Requirements

R8. The NDA methods must be applicable to all cylinder geometries in use at commercial enrichment plant (type 48 and type 30).

R9. The NDA methods must be applicable to ``fresh`` uranium as well as uranium recovered from spent fuels.

R10. Impact of the possible presence of a UF_6 deposit (0.5 mm of a different enrichment) should be kept negligible.

R11. Impact of the design variations in type 48 inches and type 30 inches should be negligible.

R12. Impact of possible heterogeneity (up to 10% of enrichment variation in particular in tails cylinders) should be minimized to the possible extend.

69

	User Requirements	Version Date:	2007-07-25
IAEA International Atomic Energy Agency	State of the art of NDA methods applicable to UF6 cylinders	Version No.:	1
Department of Safeguards SGTAU	SG-EQ-NDA-UR-0001	Page:	6 of 7

R13. Enrichment determination should be at least as accurate as attended enrichment determination by means of High Resolution Gamma Spectrometry [2]:

R13.a. Random uncertainty component, u(r): 4%.
Uncertainty component of a systematic character, u(s): 2%
Both relative for LEU products
R13.b. u(r): 8%, u(s): 5% relative for NU feed
R13.c. u(r): 15%, u(s): 10% relative for DU tails

R14. UF6 mass determination is meant to supplement the accurate figures obtained by weighing. Ideally the NDA mass determination would be accurate within:

R14.a. **10%** relative for LEU products
R14.b. **15%** relative for NU feed
R14.c. **20%** relative for DU tails

R15. Automatic interpretation of the data should not require any external information other than parameters measured by the station (e. g. weight or type of the cylinder) thus allowing unattended operation.

R16. As the measurement should not impact the industrial operation of the plant, it must be completed within 5 minutes.

5 Study Requirements

5.1 Scope

R17. The study will address all known NDA methods applicable to UF6 cylinders

R18. In case of potential application in the case a specified above, the study will report on their accuracy for enrichment determination and UF6 mass assessment.

R18.a. In the case of LEU product, NU feed and DU tails.
R18.b. Considering type 48 inches cylinders for DU and NU and type 30 inches for LEU
R18.c. Considering non homogenous filling of the cylinders in particular tail cylinders
R18.d. Considering use of recycled uranium.
R18.e. Considering deposit of UF6 of a different enrichment on the internal wall of the cylinders

R19. Further investigations will be carried out to determine the influence of the presence of UF6 cylinders in the vicinity of the measurement station and measure to be taken to minimize their impact.

R20. New techniques (e. .g active interrogation with neutron generators) or combination of techniques should be investigated as appropriate.

70

5.2   Quality

R21. Any MCNP calculations involved in the study should be carried out applying the recommendations formulated by the technical meeting on Monte Carlo simulations held in Vienna in December 2006 [3]

5.3   Documentation Required With Final Product

R22. A paper master and electronic copy in MS Word of the following documents[1] be prepared and made available to the Agency.

5.3.1   Review of existing methods

R23. Technical report stating the principles, performances, pro and cont of existing NDA methods applicable to UF6 cylinders

5.3.2   Specific investigations

R24. Specific investigations carried out on promising NDA techniques will be reported including detailed reporting on the MCNP calculations supporting conclusions

5.3.3   Cost estimate

R25. A cost estimate will be provided on NDA methods reported as potentially applicable

6   References

[1] Support Programme Task Proposal 07/TAU-04

[2] International Target Values 2000 for Measurement Uncertainties in Safeguarding Nuclear Materials

[3] Report of the Co-ordinated Technical Meeting on Numerical Modelling Concepts for IAEA held in Vienna December 2006

7   Document revision history

Revision History		
Version No.	Release Date	Description of changes
1	2007-08-09	New document.

---

[1] R22 to R25 are not required to be separate documents by must be at least addressed as separate chapters.

71

Gamma radiation detectors for safeguards applications

R. Carchon*, M. Moeslinger, L. Bourva, C. Bass, M. Zendel

International Atomic Energy Agency, Wagramerstrasse 5, P.O. Box 100, A-1400 Vienna, Austria

Available online 10 April 2007

Abstract

The IAEA uses extensively a variety of gamma radiation detectors to verify nuclear material. These detectors are part of standardized spectrometry systems: germanium detectors for High-Resolution Gamma Spectrometry (HRGS); Cadmium Zinc Telluride (CZT) detectors for Room Temperature Gamma Spectrometry (RTGS); and NaI(Tl) detectors for Low Resolution Gamma Spectrometry (LRGS). HRGS with high-purity Germanium (HpGe) detectors cooled by liquid nitrogen is widely used in nuclear safeguards to verify the isotopic composition of plutonium or uranium in non-irradiated material. Alternative cooling systems have been evaluated and electrically cooled HpGe detectors show a potential added value, especially for unattended measurements. The spectrometric performance of CZT detectors, their robustness and simplicity are key to the successful verification of irradiated materials. Further development, such as limiting the charge trapping effects in CZT to provide improved sensitivity and energy resolution are discussed. NaI(Tl) detectors have many applications—specifically in hand-held radioisotope identification devices (RID) which are used to detect the presence of radioactive material where a lower resolution is sufficient, as they benefit from a generally higher sensitivity. The Agency is also continuously involved in the review and evaluation of new and emerging technologies in the field of radiation detection such as: Peltier-cooled CdTe detectors; semiconductor detectors operating at room temperature such as HgI_2 and GaAs; and, scintillator detectors using glass fibres or $LaBr_3$. A final conclusion, proposing recommendations for future action, is made.
© 2007 Elsevier B.V. All rights reserved.

PACS: 29.40.−n

Keywords: Gamma detectors; Safeguards; HpGe; CZT; NaI

1. Introduction

The Safeguards mission of the IAEA is to provide assurance that no declared nuclear material (U, Pu, Th) is diverted to non-peaceful purposes and that no undeclared nuclear material or activities exist in States. To fulfil its mandate, the IAEA performs independent verification measurements of nuclear material using a variety of Non-Destructive Assay (NDA) instrumentation in attended or unattended mode [1]. The nature of particular inspection activities requires customization of the equipment and methods implemented: friendly and simple to use; short measurement times; and, easily portable or transportable.

High-Resolutions Gamma Spectrometry (HRGS) as well as Room Temperature Gamma Spectrometry (RTGS) are important safeguards verification tools alongside neutron detection systems, which will not be mentioned further. Moreover, the IAEA is seeking to use all available modern technology to enhance its detection capabilities.

Table 1 lists some safeguards verification activities together with the detection systems (detector, multi channel analyser, software) providing the best solution to achieve the measurement objective.

2. Detectors in current use

2.1. HpGe detectors

HRGS is performed with HpGe detectors. The detectors require liquid nitrogen (LN_2) to cool down and systems, depending upon crystal specifications, achieve a high resolution, typically in the range of 550–700 eV Full Width Half Maximum (FHWM) at 122 keV. The use of HpGe detectors is required for the intrinsic determination of Pu isotopic composition and U enrichment, relying on peak

*Corresponding author.
E-mail address: R.Carchon@iaea.org (R. Carchon).

Table 1
Safeguards verification activities

Safeguards verification activities	Applied system
Attribute testing of non-irradiated LEU and HEU	MMCA + [CZT/NaI]; HM-5
Attribute testing of non-irradiated Pu	IMCA + [(HpGe + MGA)/ (CZT + FRAM)]; HM-5
Quantitative determination of LEU, HEU or Pu hold-up	IMCA + [HpGe + ISOCS]
235U enrichment verification on uranium powders	IMCA + [(HpGe + MGAU)/ NaI]; HM-5 + NaIGEM
Determination of isotopic composition of Pu samples	IMCA + [(HpGe + MGA)/ (CZT + FRAM)]
Fresh MOX fuel attribute test	MMCA + CZT
Spent fuel attribute test	MMCA + CZT
Detection and identification of NM	HM-5 (NaI)

analysis of the 100 keV region of the gamma spectrum, utilizing MGA and MGAU software, respectively [2,3].

Spectrum acquisition is performed using the safeguard IMCA [4] spectroscopy system which integrates these two analyses.

The need to eliminate LN_2 cooling was identified, particularly for unattended systems. Manufacturers have therefore proposed systems relying on alternative cooling mechanisms based on Carnot- and Stirling-cycle cooled detection systems [5,6].

Some of the devices tested by the IAEA have not shown significant degradation in resolution; however, their reliability and adequacy of use still has to be proven.

2.2. CZT detectors

The standard (Cadmium Zinc Telluride) CZT detectors are of the semi-hemispheric type, based on a special arrangement of a pixilated anode facing a full opposite side electrode on a quasi-hemispheric detector (height = 1/2 edge). This arrangement brings an optimal electric field distribution in the crystal that allows single (electron only) charge collection. This technology yields good spectrometric performances and is simple and very robust. Due to intrinsic limitations CZT detectors with a volume less or equal to $500\,mm^3$ are mainly used for RTGS safeguards applications.

The CoPlanar Grid (CPG) CZT detector uses larger crystals and the well-known Frisch Effect to separate the features of collecting charges and generating the signals. Recently, Los Alamos National Laboratory has developed the coplanar grid technology and eV Products has produced several experimental detectors. In this design, a network of interleaved electrodes on one side of the crystal is connected to two different potentials. The CPG technology provides improved efficiency and peak shapes but is limited by its complexity and cost, in addition to the difficulty of producing large CZT crystals. Performance tests concluded that the CPG technology does not

represent a breakthrough compared to the standard IAEA hemispheric reference detectors [7].

The capture (CAP) CZT detector technology proposed by eV Products is only applicable to small crystals and represents an extension of the hemispheric concept. It consists of a special arrangement of the electrodes on all the crystal faces, having the charge collection performed as with a Frisch Grid but using cubic rather than quasi-hemispheric crystals. This tends to improve the relative efficiency of the detector at high energies. The performance evaluation conducted by the IAEA concluded, however, that the CAP technology is more sensitive to temperature operation and did not therefore represent a significant improvement in comparison with standard IAEA detectors [7].

Additional CZT detector designs are currently under review. For example, a thick CZT with dedicated pulse processing technology and special arrangements of electrodes to optimize the collection of single carrier (electrons) charges. Such a configuration utilizes an additional dedicated electrode devoted to electrical field screening (similarly to a Frisch Grid) in order to limit the charge trapping in the crystal. Pulse processing is based on a biparametric analysis (energy as a function of amplitude and collection time) [8]. A development project for this technique has been set in progress [9], with the goal of manufacturing a detector (OMEGA) with a $1000\,mm^3$ CZT crystal.

The comparative performances of gamma detectors with an emphasis upon large CZT detectors, as investigated, are given in Table 2.

2.3. NaI(Tl) detectors

The NAID has a high efficiency but features a low resolution, and requires gain stabilization. The standard NaI detectors (NAID) used by the Agency in conjunction with MMCA or IMCA acquisition hardware have an embedded 241Am stabilization source and a thermistor.

The hand-held HM-5 is a portable stand-alone instrument widely used for inspection purposes (NaI crystal 1 in. × 1 in.), with various functions, including isotope identification and attribute verification for 235U, 238U, Pu, Th and Am. Energy stabilization is achieved with a small 137Cs source (500 Bq, exempted). LED stabilization is also under development, which would provide the advantage of a source-free device [10].

3. Other detection systems

3.1. Peltier-cooled CdTe

Peltier cooling to temperatures down to −35 °C can be applied to room temperature CZT or CdTe:Cl crystals, to reduce the leakage current and consequently to improve the energy resolution of the detector. The small thickness

2/4

73

Table 2
Performances of the different types of detectors

Detector type	Volume (mm³)	ER @ 59 keV (keV)	ER @ 122 keV (keV)	ER @ 662 keV (keV)	ER @ 1408 keV (keV)	RE @ 662 keV (%)	RE @ 1408 keV (%)
HpGe	15 × 1000	0.45	0.55	1.1	N/A	200	N/A
CZT500	500	5.4	6.7	12.9	21.5	100	100
CZT1500	1690	13.2	10.7	17.5	30.0	349	178
CPG A2250	590	7.7	8.7	20.1	48.4	62	92
CPG A2317	1690	7.2	9.8	26.5	42.1	376	169
CAP 2156	500	2.5	4.2	13.0	20.2	31	27
CAP A2157	1125	7.0	8.3	20.1	33.4	76	29
OMEGA	1000	N/A	7.5	8.6	18.3	≥250	≥250
NaI(Tl)	2 in. × .5 in.	6.25	12.5	46.5	N/A		
LaBr₃:Ce	1 in. × 1 in.	6.7	8.5	21.2	N/A		
LaCl₃:Ce	1 in. × 1 in.	8.2	10.0	27.8	40.5		

Remarks:

(1) ER energy resolution is quoted at various energies.
(2) CZT500, CZT1500 are distributed by eV Products (USA).
(3) Relative efficiency RE is relative to CZT500 efficiency.
(4) The results related to the OMEGA detector are from the manufacturer.

of the PIN CdTe crystal ($\sim$2 mm, 100 mm² in area) limits its application to low energies.

Planar technology and pulse processing are used to transform the signals into usable spectra. An improved sensitivity, achieved by enlarging the crystal surface, would make the detector attractive for U or Pu verification provided that the energy resolution was not affected and a high reliability was maintained.

The Agency has supported the development and improvement of Peltier-cooled detectors from the Petersburg National Physics Institute (PNPI), which resulted in the commercial production of a battery-powered device [11].

Performance evaluation reported accurate ^{235}U enrichment determinations using a variant of the MGAU code in the 2–90 wt% ^{235}U range [12]. A recent in-house evaluation showed that spectra taken of Pu samples can be successfully processed to determine their isotopic composition with the help of the FRAM 4.2 software [13]. Both reports, however, express strong concerns about the reliability of the device and its sensitivity to microphonics. Peltier-cooled CdTe detectors have the potential to determine Pu isotopic composition of non-irradiated Pu powders or Fresh MOX fuel [13].

3.2. HgI₂ detectors

Mercury Iodine (HgI₂) is a semiconductor material with a high density (6.3 g/cm³) and a wide band gap (2.13 eV). HgI₂ crystals exhibit a very high photoelectric effect and high full-energy peak efficiency but unfortunately exhibit a low mobility of electrical charges that limit their application to low count rate (few kcps) leads due to long collection times. In addition, the effective thickness of the crystal remains low (1–3 mm) because of large charge

trapping effects. For the time being, these drawbacks make the HgI₂-based detectors unsuitable for safeguards applications. Nevertheless, their unique intrinsic characteristics should lead to further research and development efforts to provide systems suitable for safeguards applications.

3.3. GaAs detectors

Gallium Arsenide (GaAs) is the only room temperature semiconductor material with high mobility of the charges (e.g., for electrons approximately 7000 cm² V^{-1} s^{-2}) and wide band gap (1.4 eV). A combination of these two characteristics leads to potential high-performance gamma spectrometry. However, the low resistivity of GaAs (5×10^7 W/cm) does not allow applying high bias and thus limits their energy resolution.

A variety of GaAs detectors have been proposed for X-ray imaging applications [14]. The main limitation imposed on this detector technology is the difficulty in obtaining spectrometry-grade bulk GaAs material. In addition, due to their poor resistivity, only thin detectors can perform spectrometric measurements. This limits the application of such detectors to low energy measurements.

However, the possibility of a technological breakthrough might come from the development of ternary material, which might solve the problem of resistivity. Current projects are researching the possibility of cooling GaAs detectors using the Peltier Effect to achieve higher resistivity.

3.4. Lithium silicate glass fibre detectors

Cerium-doped scintillating fibres composed of lithium–silicate glass are the centre of a development effort in producing a detector of sufficient sensitivity to search for

3/4

74

undeclared materials [15]. The fibre detectors are arranged in a backpack container for portability, and provide sensitivity to gamma and neutron radiation to search for U and Pu. Tests have shown that there was insufficient discrimination between gamma and neutron radiation, raising doubts about the origin of the radiation.

3.5. LaBr₃ and LaCl₃ detectors

Recent developments revealed LaBr₃ to be a valuable scintillator for RTGS, combining an improved sensitivity and resolution when compared to NaI(Tl) [16]. Prototypes have been made available, and testing undertaken, which confirmed the improved quality. However, limitations remain, such as the high cost and temperature instability, similar to that observed in NaI(Tl) systems.

Experience has shown that LaBr₃ offers better performance than LaCl₃ in terms of resolution, even in comparison to NaI(Tl).

4. Conclusion

Several new technologies for improving gamma spectrometry instruments have been developed and tested using Member State Support Programme tasks, research contracts and in-house efforts. One of the main concerns of the IAEA is the matching, within the measurement time available during inspection, of the sensitivity and the resolution of the gamma ray detector with its intended applications.

Electrically cooled HPGe detectors are considered to eliminate the need for LN₂ cooling, especially for unattended measurement systems.

The main factor that limits the tested CZT technologies is the lack of availability of large crystals and unfortunately none of the tested prototypes have performed significantly better than the reference CZT500 and CZT1500 detectors. The quoted superior performance of the OMEGA prototype needs to be validated. The Peltier-cooled CdTe detectors have an adequate resolution to perform the measurement of Pu samples using FRAM, and could, if proven sufficiently reliable, replace HpGe detectors in certain applications.

The NaI(Tl) technology is the RTGS workhorse of the Agency and no significant further development is foreseen in this technology. LaBr₃ detectors appear to be very promising with regard to sensitivity and resolution and will be steadily followed up in terms of cost/benefit by the Agency.

The development of HgI₂ and GaAs has not yet achieved results consistent with the requirements of safeguards applications. Glass fibre detectors require further development for a sufficient discrimination between gamma and neutron signals to be achieved.

Besides the current detector technologies reviewed in this paper, improvements to software for spectrum acquisition and analysis are also warranted. In addition to the detector types mentioned, there are other types (like LiI:Eu) under consideration that could respond positively to stringent safeguards requirements.

References

[1] International Atomic Energy Agency, Safeguards Techniques and Equipment, International Nuclear Verification Series No. 1 (Revised), August 2003.

[2] R. Gunnink, A new one-detector analysis method for rapid high-precision plutonium isotopic measurements, in: Proceedings of the ninth ESARDA Symposium on Safeguards and Nuclear Material Management, London, UK, May 12–14, 1987, pp. 167–171.

[3] R. Gunnink, W. Ruhter, P. Miller, J. Goerten, M. Swinhoe, H. Wagner, J. Verplancke, M. Bickel, S. Abousahl, MGAU: a new analysis code for measuring U-235 enrichments in arbitrary samples. Presented at the IAEA Symposium on International Safeguards, Vienna, Austria, March 8–14, 1994.

[4] Model 1300, Inspector 2000, "Hardware Manual," 9231618D, Canberra Industries, 800 Research Parkway, CT-06450 Meriden, USA, 2000.

[5] R. Keyser, T. Twomey, D. Upp, Performance of light weight, battery operated, high purity germanium detector for field use, in: Proceedings of 44th INNM Conference, Phoenix, July 2003.

[6] ⟨www.canberra.com/pdf/Products/Detectors_pdf/CryoCycle%20 Cryostat%20super%20spec.pdf⟩.

[7] M. Swoboda, H. Böck, Comparison of CZT Detectors for Use in Hand Held Isotope Identifiers, Atominstitut der Österreichischen Universtäten, March 2002.

[8] G. Montemont, C. Moulin, J. Isard, L. Verger, A digital pulse processing dedicated to CdZnTe detectors, in: IEEE Nuclear Science Symposium, Rome, October 16–22, 2004.

[9] L. Verger, P. Ouvrier-Buffet, F. Mathy, G. Montemont, M. Picone, J. Rustique, C. Riffard, Performance of a new CdZnTe portable spectrometric system for high energy applications, in: IEEE Nuclear Science Symposium, Portland, 2003.

[10] G. Pausch, J. Stein, N. Teofilov, Stabilizing scintillation detector systems: determination of the scintillation temperature exploiting the temperature dependence of the light pulse decay time, in: IEEE Nuclear Science Symposium, Rome, October 16–22, 2004.

[11] M. Rahman, Performance of the PNPI CdTe Detector and its implementation for the isotopic measurements of plutonium employing the FRAM4.2 software, 2002.

[12] A. Khusainov, et al., Progress report on technical contract with IAEA No. 9984/RO: Development of High Performance PIN CdTe Detectors, 2000.

[13] D.T. Vo, P.A. Russo, Nucl. Instr. and Meth 486 (2002) 813.

[14] R. Irsigler, J. Andersson, J. Alverbro, Z. Fakoor-Biniaz, C. Frojdh, P. Helander, H. Martijn, D. Meikle, M. Ostlund, V. O'Shea, K. Smith, Nucl. Instr. and Meth. A 460 (1) (2001) 67.

[15] M. Bliss, R.A. Craig, D.S. Barnett, D.S. Barnett, D.N. Anderson, Performance of a moderating neutron spectrometer that uses scintillating fibers, in: INMM Summer Meeting, 2001.

[16] A. Kuhn, S. Surti, J.S. Karp, P.S. Raby, K.S. Shah, A.E. Perkins, G. Muehllehner, IEEE Trans. Nucl. Sci. NS-51 (5) (2004) 2550.

4/4

75

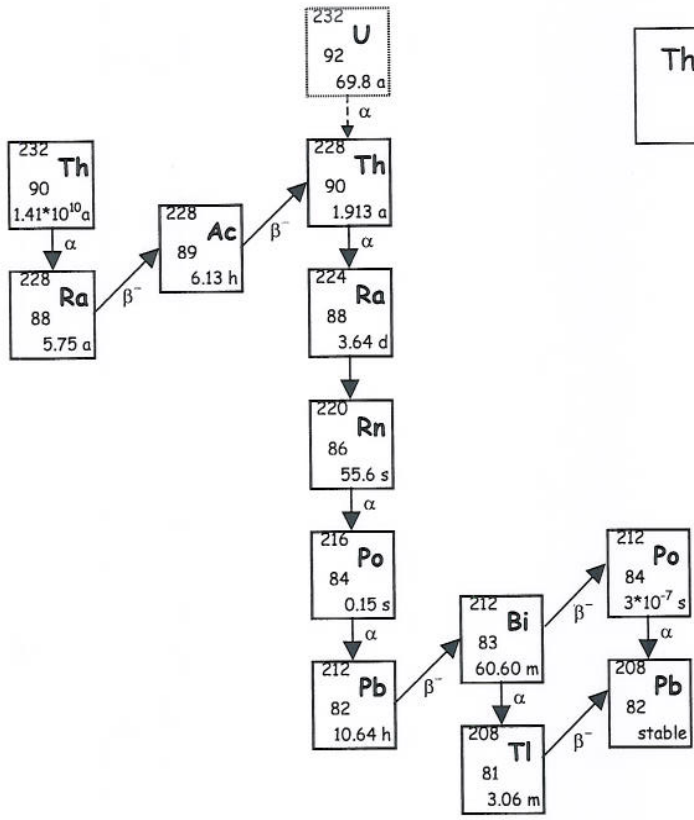# Annex 2

^{232}Th decay chain

	User Requirements	Version Date:	2007-07-25
IAEA International Atomic Energy Agency	State of the art of NDA methods applicable to UF6 cylinders	Version No.:	1
Department of Safeguards SGTAU	SG-EQ-NDA-UR-0001	Page:	2 of 7

Table of Contents

Thorium 232 decay chain
A = 4n

Neutron flux as a function of the detector position

Y48
x = 0
Natural

		1,088	0,799								0,151
		1,088	0,791								
		1,115	0,758								
		0,916	0,566								
		0,508	0,384								0,111
1,828	1,504	0,732									
0,972	0,826	0,531									
0,068		0,064									

z

r

30 60 90 120 150 180 210 240 270 300

neutron flux 1/cm² s

20 < flux
10 < flux <= 20
1 < flux <= 10
0.1 < flux <= 1
0.01 < flux <= 0.1
flux <= 0.01

Abstract

In the framework of a project aiming to establish an unattended measurement station at an isotope enrichment facility, IAEA required a study to describe the state of the art of NDA methods applicable to UF$_6$ cylinders.

The objective of the present work is to provide a feasibility assessment study of all known NDA techniques applicable to the quantitative verification of all uranium categories involved in an enrichment processing plant.

The quantification of the UF$_6$ cylinders covers:

- the determination of the enrichment,
- the confirmation the UF$_6$ mass (assumed to have been previously weighted by the plant operator and independently verified by inspectors),
- the assay of the UF$_6$ homogeneity.

The different hypothesis and practical constraints to be taken into account for the study requirements are [1]:

- the cylinders to be considered are either 30B type (product) or 48Y type (feed and tail),
- the enriched uranium is either from natural origin or reprocessed uranium,
- the cylinders must be assayed at various temperatures,
- the distance between the cylinder and the detector must be at least 50 cm to allow for safe movements of the cylinders,
- the UF$_6$ mass determination would be accurate within 10% for low enriched uranium, 15% for natural uranium and 20% for depleted uranium,
- the enrichment determination must be given with a total uncertainty which does not excess:

  - 4.5% for low enriched uranium product,
  - 9.5% for natural uranium,
  - 18% for depleted uranium,

- the measurements have to be performed in 5 minutes and in remote mode to minimize the intrusion on normal plant operator.

With the objectives and assumptions as described above in mind, this document first gives an overview of the radiation properties of UF$_6$ (chapter A) as well as some practical considerations regarding the 48Y and 30B cylinders (chapter B). The next part reviews the classical NDA methods applicable to UF$_6$ and refers to intense measurement campaigns carried out in the years 70 -80 (chapter C), whereas the chapter D is dedicated to specific studies involving more recent techniques such as analysis of delayed neutrons and delayed photons.

The most appropriate techniques will be then investigated in chapter E.
The study will be based on our own results of previous measurement campaigns (^{235}U determination with gamma detectors with germanium or LaBr$_3$ detectors) and on MCNP simulations (passive and active neutron methods).

The mission of the JRC is to provide customer-driven scientific and technical support for the conception, development, implementation and monitoring of EU policies. As a service of the European Commission, the JRC functions as a reference centre of science and technology for the Union. Close to the policy-making process, it serves the common interest of the Member States, while being independent of special interests, whether private or national.

JRC

EUROPEAN COMMISSION